Ballast shear effects on the dynamic response of railway bridges

J. Chordà-Monsonís[a,b,*], A. Romero[a], E. Moliner[b], P. Galvín[a,c], M.D. Martínez-Rodrigo[b]

[a] *Escuela Técnica Superior de Ingeniería, Universidad de Sevilla, Camino de los Descubrimientos s/n, ES-41092 Sevilla, Spain*

[b] *Universitat Jaume I, Department of Mechanical Engineering and Construction, Avda. Sos Baynat s/n, ES-12071 Castelló, Spain*

[c] *ENGREEN, Laboratory of Engineering for Energy and Environmental Sustainability, Universidad de Sevilla, Camino de los Descubrimientos s/n, ES-41092 Sevilla, Spain*

Abstract

Single-track railway bridges are susceptible of experiencing high levels of vertical acceleration on the deck that may be dangerously accentuated at resonance. This is especially critical for short-to-medium span simply supported bridges. This problem can compromise the safety of the trains and increase the maintenance costs of the track. The main objective of this work is to investigate the influence of the ballasted track on the dynamic behaviour of these structures. The present contribution provides a detailed sensitivity analysis over a wide single-track bridge catalogue covering span lengths from 10 to 25 m and considering two common deck sructural typologies: girder-deck and slab-deck bridges. The effect of the vertical stiffness of the neoprene bearings is also evaluated. A 2D Finite-Element track-bridge interaction model is implemented and used to analyse the effect of the track on the modal parameters, harmonic response and vertical acceleration of the bridges under train passages. Additionally, the weak coupling exerted by the track is studied for structures with an increasing number of consecutive spans. The results obtained reveal a notable influence of the mobilised ballast shear transfer mechanism on the dynamic response of the structures, especially for the shortest girder bridges. Finally, a track-bridge interaction model of an existing short girder bridge from a conventional railway line is updated and used to predict the experimental response measured under operating conditions. The adequacy of the numerical tool and influence of the ballast shear parameters on the dynamic response are shown.

Keywords: Railway bridges, ballast shear mechanisms, vertical acceleration, track-structure coupling, resonance, experimental measurements.

*Corresponding author.
Email address: chordaj@uji.es (J. Chordà-Monsonís)

1. Introduction

The need for personal and freight mobility around the world has increased dramatically in recent decades. Along with it, transportation systems have experienced a sustained development. In particular, railway transport has proved to be essential for the development of modern societies, due to its numerous advantages such as high transportation capacity, competitive travelling times, adequate levels of security and comfort for the passengers and its potential as a sustainable way of mobility.

For the European Union, the establishment of a single European railway space is a long-term strategic priority [1]. Thus, it is fair to expect a progressive increase in the number of railway lines, the number of trains, the transportation capacity of the vehicles and their operating speeds. In terms of design, monitoring, and maintenance, this constitutes a challenge for the infrastructures, which will have to operate under more demanding conditions while fulfilling the required levels of quality, security and reliability. In the case of the Spanish network, it is structured along 16000 km of operating lines, of which 3000 km are High Speed (HS) lines [2]. In total, more than 6000 bridges are part of the railway system.

The dynamic effects on railway bridges are considered of major interest and concern for scientists and engineers, especially since the opening of the first HS lines [3], as these phenomena generally aggravate with increasing velocities. According to Eurocode (EC), the verification of maximum peak deck acceleration shall be regarded as a traffic safety requirement checked at the serviceability limit state for the prevention of track instability. The maximum acceleration is limited to $3.5\,\mathrm{m/s^2}$ in ballasted track bridges and to $5\,\mathrm{m/s^2}$ in slab-track bridges [4, 5], and these two limits are related to the possible deconsolidation of the ballast and to the risk of losing wheel-rail contact, respectively. An excessive level of vertical vibrations may cause passenger discomfort, a raise in the maintenance costs of the track, the premature deconsolidation of the ballast layer and the resulting misalignment of the rails in ballasted track bridges, a possible loss of contact between the wheels and the rails, and an increasing risk of derailment in the worst-case scenario. In this regard, single track short-to-medium span (10 – 25 m) simply-supported (SS) railway bridges are prone to exhibit important acceleration levels due to their usually associated low mass, especially at resonance [6, 7].

Train induced vibrations in railway bridges is a rather complex interaction problem affected by several factors. The most obvious ones are the geometrical and mechanical properties of the bridge, the scheme of the train axles and the circulation speed. In addition, other much more uncertain interaction mechanisms may also significantly affect the response of the bridge such as vehicle-structure, track-structure and soil-structure interaction, which are currently under investigation [8]. Moreover, the computational cost of representing accurately these interaction mechanisms is considerable and time-consuming. This is why simplified models

that often disregard them are regularly used in engineering consultancies.

This investigation is dedicated to the study of the effect exerted by the ballasted track on the vertical dynamic response of SS railway bridges. This is a matter of interest since, according to some authors, the contribution of the ballasted track on the dynamic response of the bridge is not yet fully understood [9, 10], and constitutes one of the reasons for the discrepancies found between calculated and measured modal parameters in short-to-medium span bridges [10]. Several publications can be found in the literature dedicated to the investigation of the vertical track-bridge interaction and its effect on the modal parameters and on the dynamic response of railway bridges. Among them, Liu et al. [11] compared the prediction of the dynamic response of a multi-span railway viaduct using moving loads and vehicle-bridge interaction models. The authors found that the track creates a connection between statically decoupled spans that directly affects the dynamic behaviour of the bridge and its modal properties. Chellini et al. [12] identified the modal parameters of two composite isostatic multi-span railway bridges and analysed the dynamic response under operating conditions. As a result, the authors identified a clear dynamic interaction between consecutive spans. Moreover, they pointed out the importance of including the continuous rails and the ballast layer in the numerical models to obtain a realistic representation of the dynamic response. Liu et al. [13] evaluated the influence of the weak coupling exerted by the track between consecutive SS spans on the dynamic response of the multi-span Sesia railway viaduct using two models: (i) a single-span FE model of the bridge with modified boundary conditions, and (ii) a reduced-order model of the whole viaduct or Component Synthesis Model (CMS). The authors concluded that the CMS technique offered good results at reasonable computational cost, although the single-span model could be used as well to obtain an agreeable approximation of the dynamic response of the structure. Matsuoka et al. [14] studied the dynamics of the same viaduct focusing on the influence of local deck vibrations. They pointed out that high-order resonances associated to local deformation modes could cause larger accelerations than those that would be predicted by considering only global deformation modes. In addition, in relation with the work of Liu et al. [13], results in [14] highlighted that the influence of the weak coupling between adjacent spans had a negligible effect on the acceleration response of the bridge, especially at resonance. Bornet et al. [10] investigated the influence of the ballasted track in a single-span steel truss railway bridge, concluding that the track provided an additional stiffness of about $22 - 27$ % in the three lowest modes. Furthermore, they revealed that the effect of the ballast stiffness and the track continuity does not manifest significantly on the first vertical bending and torsional modes, whereas, in contrast, have an important influence on the second vertical bending mode. Seemingly, the addition of the ballast provided an extra weight on the structure that prevented the

translation of the bearings and affected significantly the stiffness for the first and third vertical bending modes. Other authors as Galvín et al. [15] presented the results of an experimental campaign carried out on five railway bridges. In this contribution, the authors investigated the load transfer between loaded and unloaded adjacent decks sharing a continuous ballast layer, and pointed out the importance of taking into account this coupling effect.

The work presented herein is driven by the results obtained in a preliminary study by the authors [16], in which a high dispersion was detected in the values employed for the track parameters in the literature, even for similar track infrastructures. Additionally, a sensitivity analysis was carried out on the vertical stiffnesses and damping of the rail pads and the ballast. The results proved that these parameters affected the response of the bridge mainly at resonance, but still, the influence of these parameters was very small compared to the ballast shear transfer mechanisms. The present contribution aims to go further and broaden the focus with respect to previous contributions. To this end, three main objectives are defined to investigate how the presence of the ballasted track affects the dynamic response of railway bridges: (i) to evaluate the influence of the main track parameters on the modal properties and on the harmonic and dynamic response of the bridges; (ii) to analyse the weak coupling effect exerted by the continuity of the ballasted track between successive spans in the vertical acceleration response under railway traffic and, additionally, to check the adequacy of models that disregard this effect; and (iii) to assess the suitability of simplified discrete track-bridge interaction models to predict the response of real structures.

The main novelty of this paper is the definition of a vast bridge catalogue of single-track multi-span bridges that is meant to cover some of the most representative bridge typologies found in the European railway network for span lengths from 10 to 25 m: girder and slab bridges [17]. This represents an important newness, since previous publications usually focus on particular case studies, which prevents the derivation of general conclusions. Girder bridges are structures with precast decks composed of concrete slabs resting on pre-stressed longitudinal girders with or without transverse diaphragms at the supports. Slab bridges are made up of solid or voided concrete slabs, filler beams encased in concrete pseudo-slabs, etc. Other typologies found in short-span bridges such as prefabricated twin box girder decks or portal frames are less prone to experience vibration problems due to their inherently higher stiffness or damping, and are not included in the study. A 2D Finite-Element (FE) track-bridge interaction model including a three-layer discretisation of the track, based on that proposed by Zhai et al. [18], is implemented and used to perform an extensive sensitivity analysis to accomplish the three aforementioned objectives.

Among the particularities of this study, it is worth mentioning that the results are obtained for the

structures at resonance but also at non resonance and cancellation situations. Plus, the solution for the dynamic problem is obtained through direct integration of the equations of motion using the full FE model (i.e., modal superposition is not applied to avoid its associated simplifications). In addition, objective (i) is meant to fill a gap of knowledge that could lead to a better undertsanding of the dynamic problem in railway bridges. Objective (ii) adresses the problematic of simplified single-span models, which are widely used in engineering consultancies and due to the weak coupling exerted by the ballast, they may not be able to predict the maximum vertical response of a multi-span structure. Finally, regarding objective (iii), a numerical-experimental comparison is performed on a short girder bridge from a Spanish conventional railway line under operating conditions and the influence of the ballast shear parameters on the fitting of the response is shown.

This paper is organised as follows. In section 2, the bridge catalogue is presented and the FE track-bridge interaction model is described in detail. In section 3, a sensitivity analysis is carried out and the influence of the track parameters on the natural frequencies and on the harmonic response of the bridges under study is evaluated. Additionally, the dynamic response of multi-span bridges under the passage of trains and the influence of certain track parameters at resonance, cancellation and other conditions is analysed. In section 4, the weak coupling exerted by the continuity of the track is investigated in bridges with an increasing number of spans. In section 5, experimental measurements on a two-span conventional bridge are compared to numerical predictions, and eventually, in section 6, the main conclusions are summarised.

2. Bridge catalogue and numerical model

2.1. Bridge catalogue definition

A representative catalogue of single-track SS railway bridges is defined covering short-to-medium span lengths, since these are the most susceptible to experience high vertical acceleration levels under operating conditions. The span lengths of interest vary from 10 to 25 m, and they have been studied in 2.5 m intervals. For each length, two common typologies are considered: (i) girder bridges (i.e. pre-stressed concrete girder decks); and (ii) slab bridges (i.e. solid or voided concrete slabs, filler beam pseudo-slabs, etc.), as shown in Fig. 1. As for the deck vertical supports, infinitely rigid supports (SS) and elastic supports (ES) accounting for the vertical flexibility of laminated neoprene bearings are differentiated. Only this type of bearing is considered as (i) it is widely used for simply-supported, short-to-medium span length railway bridges [19] and (ii) it is an adequate solution used to absorb small horizontal displacements of the bridge deck at the supports as the ones expected in railway bridges under normal operating conditions according to

the Spanish and European standards [5, 20]. Other types of bearings, capable of absorbing much higher horizontal displacements, such as lead rubber bearings or friction pendulum bearings are usually found on longer bridges located in highly seismic zones and are out of the scope of this paper, as it is not intended to evaluate seismic action on the structures considered.

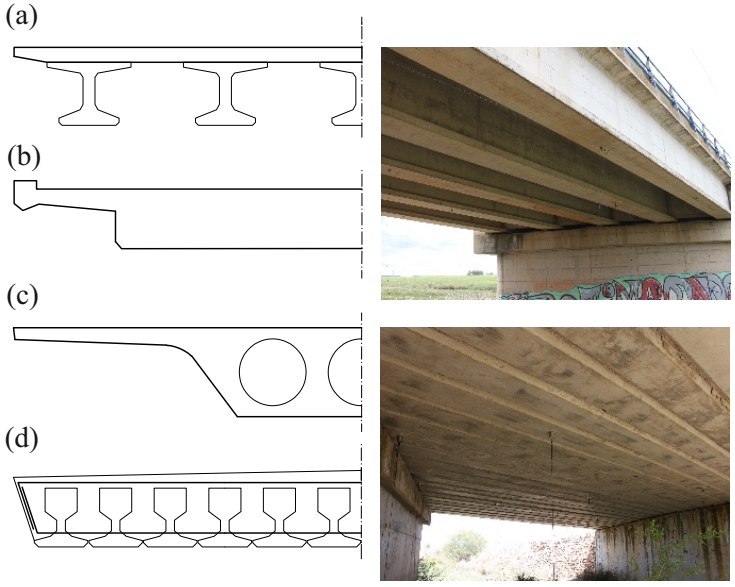

Figure 1: Left: (a) pre-stressed concrete girder deck; (b) solid concrete slab; (c) voided concrete slab; (d) filler beam pseudo-slab. Right: photographs of a girder deck (top) and a pseudo-slab deck (bottom) in Madrid-Sevilla HS line.

Fig. 2 shows, for the 28 bridges of the catalogue, the total mass of the deck per span M_{bi} and the fundamental frequency f_1. These values are selected on the basis of the study performed by Doménech et al. [21]. For the girder decks, the mass of reported single-track existing bridges approaches the inferior limit in Fig. 2(a). This limit is selected because, additionally, corresponds to the most unfavourable case for the acceleration criterion. The fundamental frequency for this typology is selected as 50% of the difference between the EC [5] limits for application of the simplified method, based on the data of the bridges presented in reference [21].

As for the slab decks, the mass is selected as 25% of the difference between the upper and lower limits for each length. This corresponds to an average value for the mass of existing single-track slab bridges. Regarding the fundamental frequency for this typology, the same criterion is applied. Finally, an ES version of each deck is also defined admitting that the ratio κ between the bridge bending stiffness and the supports vertical stiffness equals approximately 0.05, as shown in Eq. 1, which leads to a reduction in the fundamental frequency less than 3% with respect to the SS case, as indicated in [17]. This value is considered a reasonable

averaged flexibility ratio to be expected in the structures under consideration which usually rest on neoprene bearings. Other types of elastic supports, such as pot bearings, which are more frequent in longer spans, offer higher vertical stiffness than neoprene bearings. Therefore κ=0.05 can be seen as an upper limit for these cases.

In Eq. 1, $E_{bi}I_{ybi}$ stands for the bridge bending stiffness, while $\bar{K}^{n}_{bi,dyn}$ indicates the vertical stiffness of the neoprene bearings for dynamic loads and L_{bi} the span length.

$$\kappa = \frac{E_{bi}\, I_{ybi}\, \pi^3}{\bar{K}^{n}_{bi,dyn}\, L^3_{bi}} \approx 0.05 \tag{1}$$

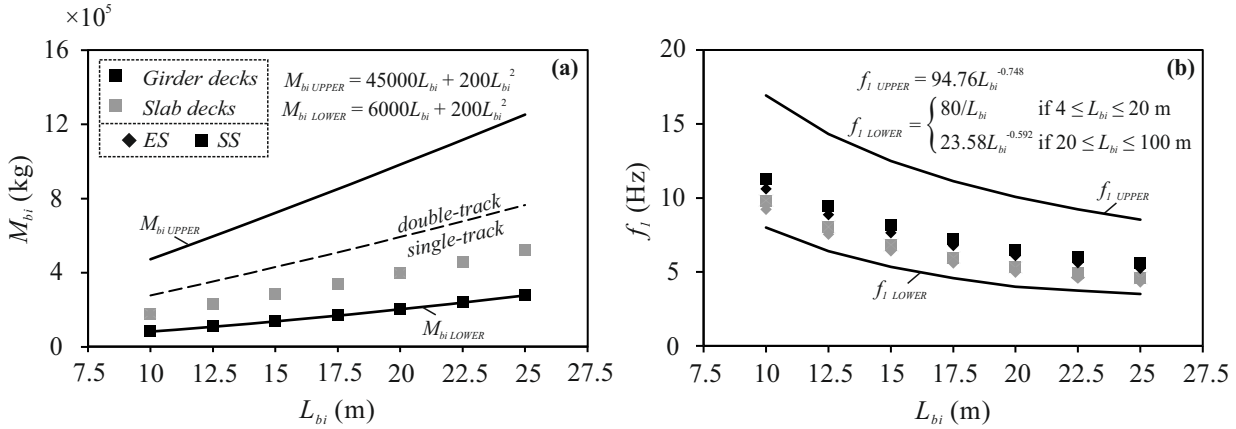

Figure 2: (a) Mass per span and (b) fundamental frequency of the bridges under study. Mass and frequency limits selected according to [21] and [5], respectively.

In Tables 1 and 2, the mechanical properties for the girder and the slab bridges of the catalogue are included. Additionally, an identification code is assigned to each bridge according to these characteristics (e.g. the GD-ES-10 bridge corresponds to a girder deck bridge, with elastic supports and 10 m of span length).

L_{bi} [m]	f_1 [Hz]	M_{bi} [kg]	$E_{bi}I_{ybi}$ [MNm^2]	$\bar{K}^n_{bi,dyn}$ [MN/m]	Designation
10	11.28	80000	3556	∞	GD-SS-10
	10.61	80000	3178	3124	GD-ES-10
12.5	9.42	106250	6449	∞	GD-SS-12.5
	8.86	106250	5808	2868	GD-ES-12.5
15	8.14	135000	10600	∞	GD-SS-15
	7.65	135000	9631	2698	GD-ES-15
17.5	7.21	166250	16440	∞	GD-SS-17.5
	6.77	166250	14970	2578	GD-ES-17.5
20	6.48	200000	24140	∞	GD-SS-20
	6.09	200000	22020	2492	GD-ES-20
22.5	5.99	236250	35050	∞	GD-SS-22.5
	5.63	236250	32030	2494	GD-ES-22.5
25	5.58	275000	49270	∞	GD-SS-25
	5.25	275000	45110	2504	GD-ES-25

Table 1: Mechanical properties of girder bridges.

L_{bi} [m]	f_1 [Hz]	M_{bi} [kg]	$E_{bi}I_{ybi}$ [MNm^2]	$\bar{K}^n_{bi,dyn}$ [MN/m]	Designation
10	9.80	177500	6628	∞	SD-SS-10
	9.22	177500	6063	4671	SD-ES-10
12.5	8.03	228125	10910	∞	SD-SS-12.5
	7.55	228125	9971	4028	SD-ES-12.5
15	6.83	281250	16600	∞	SD-SS-15
	6.43	281250	15290	3588	SD-ES-15
17.5	5.97	336875	24010	∞	SD-SS-17.5
	5.61	336875	22060	3268	SD-ES-17.5
20	5.30	395000	33190	∞	SD-SS-20
	4.99	395000	30540	3027	SD-ES-20
22.5	4.91	455625	46910	∞	SD-SS-22.5
	4.61	455625	43230	2987	SD-ES-22.5
25	4.58	518750	64090	∞	SD-SS-25
	4.31	518750	59470	2958	SD-ES-25

Table 2: Mechanical properties of slab bridges.

2.2. Track-bridge interaction model

A 2D FE track-bridge interaction model is implemented for subsequent analyses (see Fig. 3). The decision of using a planar model is based on the following: (i) the main interest are the vertical vibrations induced by railway traffic. Lateral vibrations, which may be relevant in the case of viaducts with high piers in combination with wind loads, curved bridges or multi-track decks with eccentric traffic [22], fall out of the scope of this study; (ii) the bridges under study are straight single-track bridges and the track is centered in the deck width. Consequently, the contribution of modes different from the longitudinal bending ones (torsion or transverse bending modes, typical in multi-track or skewed bridges) is not expected to be relevant at low frequencies; (iii) it is intended to cover a vast catalogue of bridges considering different span

lengths, linear masses, fundamental frequencies, and boundary conditions. Therefore, computational time is a relevant factor and using a planar model for this application is considered appropriate.

The track is simulated by means of a three-layer discrete model based on the one proposed in reference [18], and couples a series of elastically supported bridge spans. From top to bottom, E_r, I_{yr} and m_r stand for the rail Young modulus, cross-section moment of inertia with respect to the Y axis, and linear mass. Below, the vertical damping and stiffness of the rail pads, C_p and K_p, of the mobilised ballast, C_b and K_b, and of the subgrade C_f and K_f, are included at the sleepers locations. Also, to account for the continuity and the coupling effects of the interlocking ballast granules, a couple of linear shear stiffness K_w and shear damping C_w is introduced connecting the vertical displacement of adjacent ballast masses. The lumped masses M_{sl} and M_b stand for the mass of each sleeper and the vibrating mass of ballast under a sleeper support, respectively. Regarding K_f^b and C_f^b, they correspond to the subgrade stiffness and damping on the bridge deck, which in this study are set to $100 \times K_f$ and 0, respectively, admitting that the ballast rests directly on the slab. As indicated in Fig. 3, the rail and track parameters are multiplied by a factor of two, as only one rail is explicitly included in the model. The track model admits Ahlbeck hypothesis [23], which states that the load transmitted from a sleeper to the ballast approximately coincides with a cone distribution with an inclination defined by the ballast stress pervasion angle corresponding to the Poisson's ratio.

As per the bridge, it is represented by N_{sp} isostatic uniform Bernoulli−Euler (BE) beams, where N_{sp} stands for the number of spans. In the present work, N_{sp} is set to a value of 2, as two identical spans are considered for each bridge, except in section 4, where the influence of the track weak coupling is evaluated in bridges with a different number of spans. The laminated rubber bearings of the bridge are represented as vertical linear springs in the numerical model. Therefore, their vertical stiffness is introduced through the constant equivalent vertical dynamic stiffness $\bar{K}_{bi,dyn}^n$ at each end section of the i-th bridge span (e.g. the sum of the individual bearing stiffnesses at each support). The parameters L_{bi}, E_{bi}, I_{ybi} and m_{bi} correspond to the length, the Young modulus, the cross-section moment of inertia with respect to the Y axis and the linear mass of the i-th bridge deck, respectively. With this configuration, the vertical interaction between successive spans is only provided by the continuity of the ballasted track. In the simulations, a track length of $L_{r,prev} = 20\,\mathrm{m}$ is included before and after the bridge. This length represents more than 30 times the sleeper distance D_{sl}, which is adequate attending to previous studies [24, 25]. The track model used in this work focuses on the vertical interaction of the track-bridge system, while the longitudinal interaction is neglected. In the absence of braking forces or temperature gradients, the coupling effects in the vertical

direction prevail over those in the longitudinal direction, and thus they may be evaluated in a decoupled manner [26, 27]. This is consistent with recent publications devoted to transverse vibrations in railway bridges [22, 28, 29].

Moreover, the track longitudinal stiffness is very high when compared to the vertical stiffness of the track-bridge systems. In addition, the natural frequencies of the modes that mobilise a significant amount of mass in the longitudinal direction exceed the maximum frequency of interest of 30 Hz related to the destabilization of the ballast layer associated with vertical vibrations according to EC. This fact has been verified by means of a modal analysis performed with a detailed 3D numerical model of an existing railway bridge implemented for this purpose in ANSYS(R)17.1. The model, similar than the one proposed in [30], considers a continuous discretisation of the ballasted track with solid FE, and reproduces with reasonable accuracy the first 5 experimentally identified natural frequencies and mode shapes of Old Guadiana bridge, an existing structure that belongs to a conventional railway line in Spain. This bridge corresponds to the case study that is documented in section 5 of this paper. A comprehensive modal analysis was carried out considering frequencies up to 200 Hz, with the aim of detecting modes with a significant deformation of the track with respect to the slab in the longitudinal direction (X). The results of the numerical simulations showed that modes with a high participation of the track deforming in the longitudinal direction present frequencies much higher (over 100 Hz) than twice the maximum frequency of interest (30 Hz) according to EC limit.

A constant moving load model is selected to represent the train excitation, therefore neglecting vehicle-structure interaction effects (VBI). The reasons for this are: (i) it is intended to isolate the effect of the track components affecting the dynamic response of the bridge in order to investigate their separate influence; (ii) it is an objective of this work to determine the adequacy of this type of models, as they may be useful and valuable in engineering and technical consultancies; and (iii) as indicated in references [21, 31], the effects of the VBI when the track is included are relevant mainly at resonance. Track irregularities are not included as, despite they have a noticeable contribution on the vertical response of the vehicle itself and are perceptible in the soil far away from the track, they are less important for the infrastructure at the bridge site [32, 33]. The adequacy of the aforementioned simplifications is justified in section 5.

As for the track parameters, an important dispersion has been detected among different publications. Based on a review presented by the authors in reference [16], those included in Table 3 are adopted now as a reference set, expressed per rail seat. M_b, K_b and K_f are calculated applying equations (2a), (2b) and (2c), respectively, according to [18]. Regarding the rail, the rail pads and the sleepers, their properties are

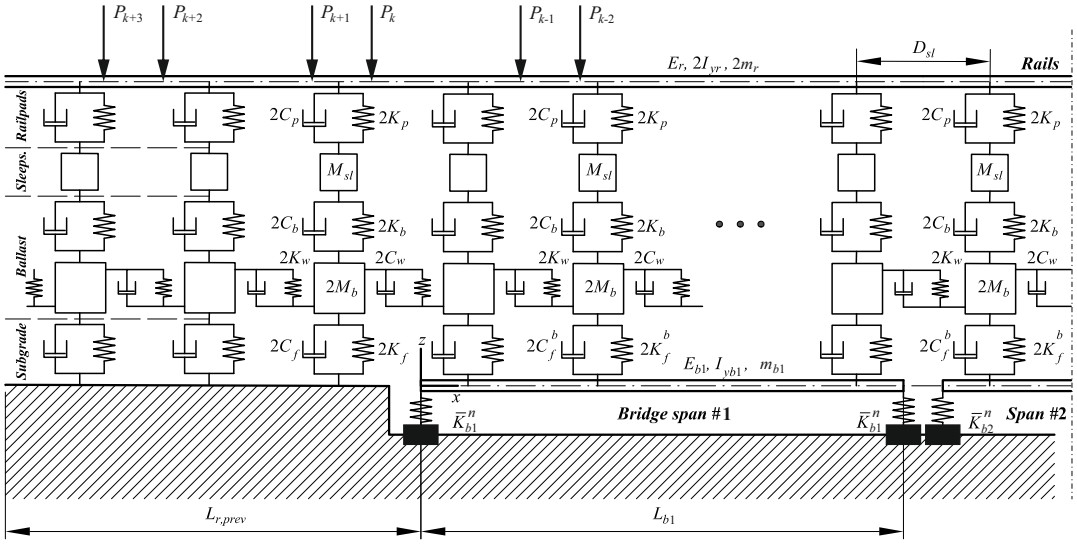

Figure 3: 2D track-bridge interaction model.

selected from Spanish and European Standards [20, 34–36].

The ballast shear stiffness K_w and damping C_w are not always included in discrete track models. The authors have found that the information about reasonable values for these parameters is scarce. References [37–41] admit the values proposed by the Chinese Railways included in the work by Zhai [18]. Only Wang et al. [42] propose a lower level of shear damping for similar track characteristics but no experimental justification is provided. In the absence of more information, the reference values used for these parameters are those proposed in reference [18]: $K_w = 7.84 \times 10^7$ N/m and $C_w = 8.00 \times 10^4$ Ns/m.

$$h_0 = h_b - \frac{D_s l - l_b}{2 \tan \alpha} \qquad M_b = \rho_b \Big[l_b h_b (l_e + h_b \tan \alpha) + l_e (h_b^2 - h_0^2) \tan \alpha + \frac{4}{3} (h_b^3 - h_0^3) \tan^2 \alpha \Big] \tag{2a}$$

$$K_b = \frac{K_{b1} K_{b2}}{K_{b1} + K_{b2}} \qquad K_{b1} = \frac{2(l_e - l_b) \tan \alpha}{ln\Big[\frac{l_e D_{sl}}{l_b (l_e + D_{sl} - l_b)} \Big]} \qquad K_{b2} = \frac{D_{sl}(D_{sl} - l_b + 2l_e + 2h_b \tan \alpha) \tan \alpha}{l_b - D_{sl} + 2h_b \tan \alpha} E_b \tag{2b}$$

$$K_f = D_s l (l_e + 2h_b \tan \alpha) E_f \tag{2c}$$

The model is implemented in ANSYS v.17.1.0. Mass, stiffness and damping matrices are exported to

MATLAB v.2017b, and the equations of motion of the full model are integrated in the time domain applying the Newmark-beta constant acceleration algorithm. The time step for numerical integration is established as the minimum between 1/50 times the smaller period of interest and 1/20 times the load travelling time between two consecutive sleepers.

Notation	Parameter	Value	Unit	Reference
E_r	Rail UIC 60 elastic modulus	2.100×10^{11}	Pa	[35]
I_{yr}	Rail UIC 60 moment of inertia	3038.3×10^{-8}	m^4	[35]
m_r	Rail UIC 60 mass per unit of length	60.21	kg/m	[35]
K_p	Rail pad vertical stiffness	1.000×10^8	N/m	[34, 36]
C_p	Rail pad damping	7.500×10^4	Ns/m	[18]
M_{sl}	Sleeper mass	300	kg	[20]
D_{sl}	Sleeper distance	0.600	m	[20]
l_e	Half sleeper effective supporting length	0.950	m	[18]
l_b	Sleeper width	0.300	m	[20]
α	Ballast stress distribution angle	35	$\circ$	[18]
h_b	Ballast thickness	0.300	m	[20]
ρ_b	Ballast density	1800	kg/m^3	[18]
M_b	Ballast vibrating mass	317.910	kg	[18]
E_b	Ballast elastic modulus	1.100×10^8	Pa	[18]
K_b	Ballast vertical stiffness	1.933×10^8	N/m	[18]
C_b	Ballast damping	5.880×10^4	Ns/m	[18]
E_f	Subgrade K_{30} modulus	9.000×10^7	Pa/m	[18]
K_f	Subgrade vertical stiffness	7.399×10^7	N/m	[18]
C_f	Subgrade damping	3.115×10^4	Ns/m	[18]
K_w	Ballast shear stiffness	7.840×10^7	N/m	[18]
C_w	Ballast shear damping	8.000×10^4	Ns/m	[18]

Table 3: Parameters of the track model, per rail seat.

3. Sensitivity analysis on modal parameters, harmonic and dynamic responses

3.1. Adopted approach: key parameters

In this section, the key parameters for this study are determined. For this purpose, a preliminary sensitivity test is carried out to evaluate how the independent variation of the track parameters affects the modal frequencies of the bridges in the catalogue. Fig. 4 shows twelve of the mode shapes present in the structures considered. Figs. 4(a-f) correspond to lower frequency global deformation modes of the bridge, while Figs. 4(g-l) represent higher modes with a predominant participation of the track. In both cases, modes appear in pairs with close frequency values (e.g., for the GD-ES-10 bridge, $f_1 = 10.61$ Hz and $f_2 = 10.66$ Hz ; $f_3 = 33.89$ Hz and $f_4 = 34.13$ Hz).

For the sake of conciseness, the results of this preliminary test are presented only for the GD-ES-10 bridge, as due to its length and natural frequency, is the most affected by the presence of the track, as will

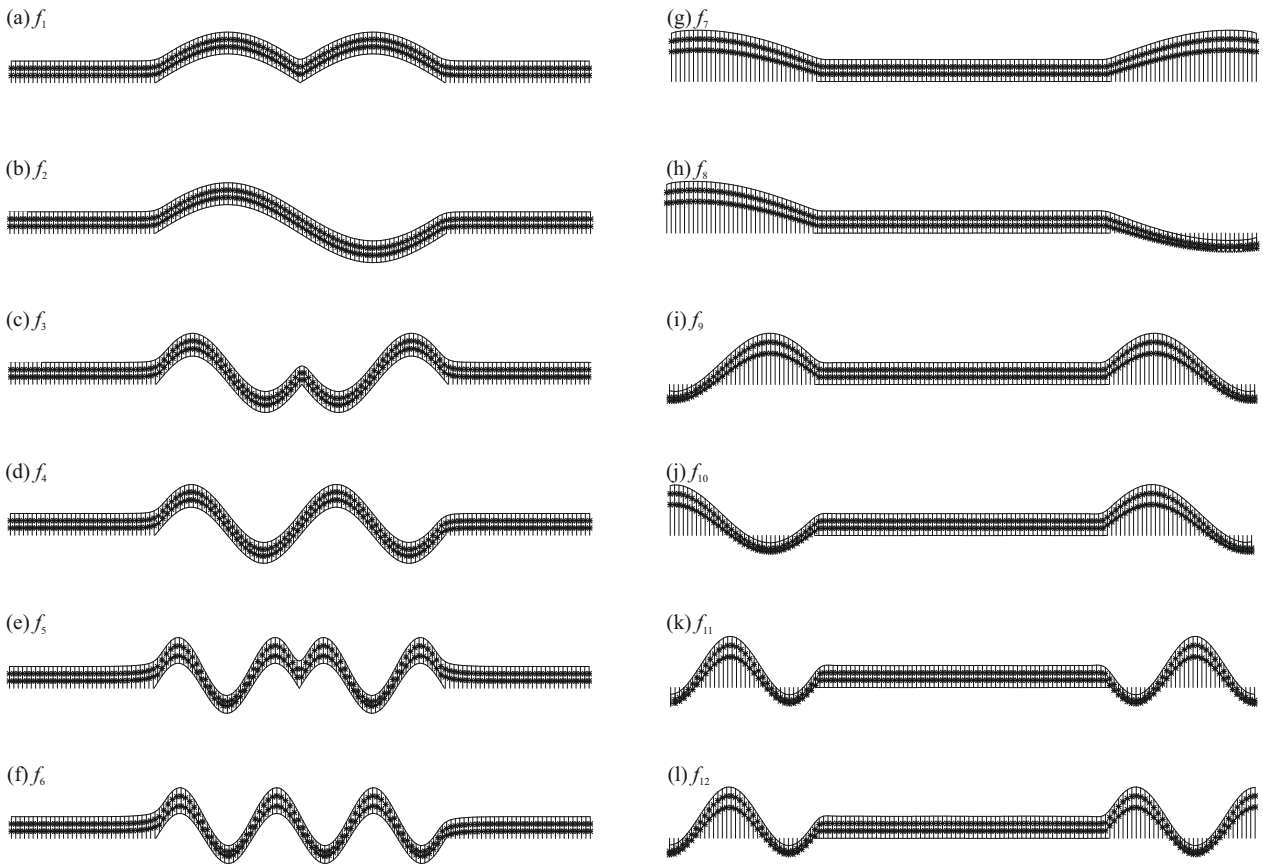

Figure 4: Left (a-f): first six modes of vibration for the bridges of the catalogue. Right (g-l): frequency modes with a clear participation of the track.

be shown later. The results for the remaining bridges exhibit the same trend. The next individual variations are applied to the stiffness of the ballast (for its shear and vertical components), subgrade and rail pads: [0.5, 1.0, 1.5, 2.0] $\times$ K_w, [0.5, 1.0, 1.5, 2.0] $\times$ K_b, [0.5, 1.0, 1.5, 2.0] $\times$ K_f, [0.5, 1.0, 1.5, 2.0] $\times$ K_p, respectively. Fig. 5 shows the alteration caused in the first and third natural frequencies of the bridge by the variations of the aforementioned track parameters. On the Y axis, the frequency variation is expressed in relation to the nominal case. A stands for the factor that multiplies the nominal value of the stiffness, while K_i stands for the stiffness of any of the track parameters. As can be seen, only the ballast shear stiffness significantly affects the natural frequencies. In this regard, a maximum frequency variation of almost 10% is reached for the first mode when K_w is doubled. The variations caused by the other parameters are negligible, all being lower than 1%. This is consistent with the preliminary conclusions presented in reference [16] for a case study and justifies the focus of this work on the ballast shear parameters and their influence on bridges of

different lengths and typologies.

Despite the obvious influence of this parameter (and of the ballast shear damping), they are often disregarded in the discrete track models presented in the literature, and their influence on the bridge dynamic response has not been investigated with generality. As stated before, in the cases where included, the values admitted for these parameters correspond, most of the times, to those calculated for the Chinese. Railways and used in the work presented by Zhai et al. in reference [18]: $K_w = 7.84 \times 10^7\,\mathrm{N/m}$ and $C_w = 8.00 \times 10^4\,\mathrm{Ns/m}$.

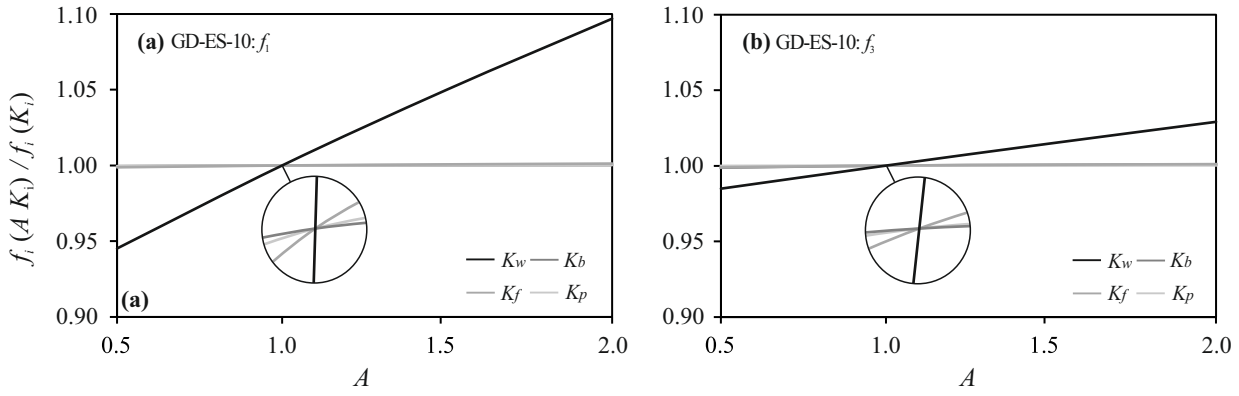

Figure 5: Natural frequency variations for GD-ES-10 bridge with track parameters K_w, K_b, K_f and K_p.

For the previously said, in what follows, the influence of the ballast vertical shear coupling effect is investigated over the bridges of the catalogue. Subsection 3.2 adresses the influence of the ballast shear stiffness in the modal parameters. The effect of the ballast shear stiffness and damping on the bridges harmonic response is evaluated in subsection 3.3 and the dynamic response of the structures under train passages is analysed in subsection 3.4

3.2. Influence of K_w on the modal parameters of the bridges

In this section, the influence of the ballast vertical shear stiffness K_w on the bridge normal modal parameters is evaluated. Because of the natural frequencies of the bridges appearing in pairs, the first, third and fifth longitudinal bending modal frequencies are determined for variations of the ballast shear stiffness: [0.0, 0.5, 1.0, 1.5, 2.0] $\times$ K_w. Fig. 6 shows the results for all the bridges in the catalogue. The results are grouped per bridge length. Each graph shows the variation in the natural frequency f_i for $i = 1, 3, 5$ relative to the reference case $1.0 \times K_w$.

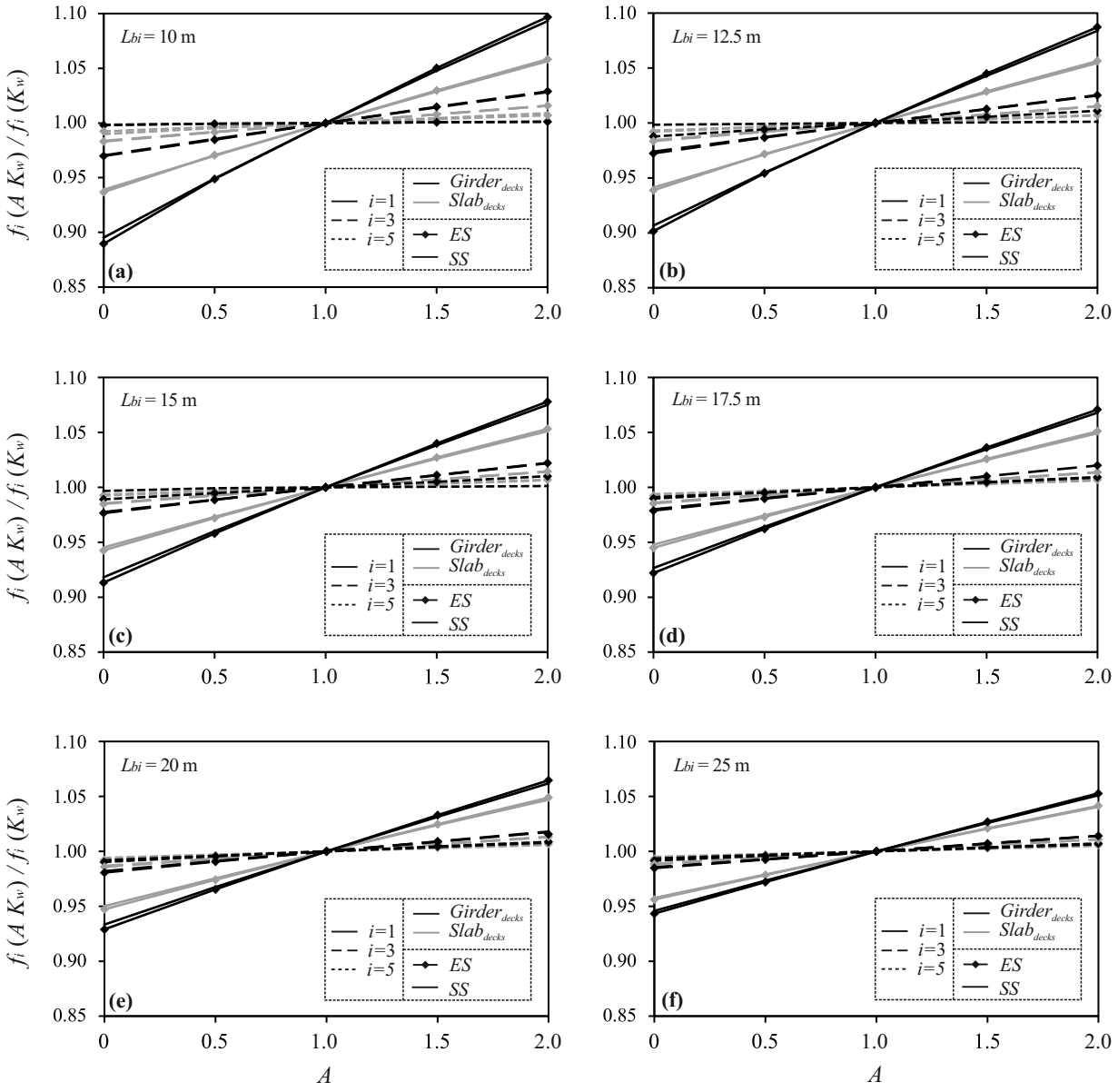

Figure 6: Variation of f_1, f_3 and f_5 with respect to the frequency in the nominal case **as a** function of K_w.

The following is observed:

- Natural frequencies increase with K_w. Bridges with the shortest spans in a certain typology are the most affected by the variation of this parameter.
- The fundamental frequency f_1 corresponding to the first longitudinal bending mode is significantly more affected than higher frequencies. The effect of K_w reduces with increasing frequencies.

- Regarding the typology, girder bridges, with lower longitudinal bending stiffness, are affected to a higher extent than slab bridges.

- As per the bridge supports, elastically-supported bridges are slightly more affected by K_w than simply-supported bridges. Nevertheless, the difference is not relevant, especially for modes higher than the fundamental one.

These results are consistent throughout the bridge catalogue. Short-span elastically-supported girder-deck bridges are the most sensitive ones to the variation of K_w. On this matter, the maximum frequency ranges of variation for the first, third and fifth modes obtained are 20%, 6% and 3%, respectively, for the shortest girder bridge considered (GD-ES-10), and 11%, 3% and 1.5%, respectively, for the longest one (GD-ES-25).

3.3. Influence of K_w and C_w on the harmonic response of the bridges

In this section, the influence of the ballast shear stiffness and damping on the harmonic response of the bridges is analysed. A vertical harmonic force with amplitude $F_0 = 210\,\text{kN}$ is applied to the rail in the center of the first span. The maximum absolute vertical displacement of the rail in the same section is determined for forcing frequencies in the range $f_f \in [1{,}250]$ Hz in steps of $\Delta f_f = 0.01$ Hz. This wide frequency range has been chosen to properly capture at least the resonant response of the lowest structural modes in frequency order with high participation of the track, although European Standards [4] limit the maximum frequency of interest for the verification of the Serviceability Limit State for traffic safety up to the greater of (i) 30 Hz, (ii) 1.5 times the frequency of the fundamental mode of vibration or (iii) the frequency of the third one. The analysis is repeated for individual variations of the ballast vertical shear stiffness and damping of [0.0, 0.5, 1.0, 1.5, 2.0] $\times$ K_w and [0.5, 1.0, 1.5, 2.0] $\times$ C_w, being C_w and K_w the reference values of these parameters (see Table 3).

In Fig. 7, results of the harmonic analysis are represented for each bridge length. In Figs. 7(a-d) and in Figs. 7(e-h), individual variations of K_w and C_w are applied, respectively. For the sake of brevity, only the results for the ES girder bridges are presented in this section for $L_{bi} = 10, 15, 20$ and $25\,\text{m}$, as no relevant differences were detected in the trends between typologies or support conditions. No structural damping is added apart from that of the discrete track elements. The rail is discretised into two beam elements between consecutive sleepers, and so are the bridges.

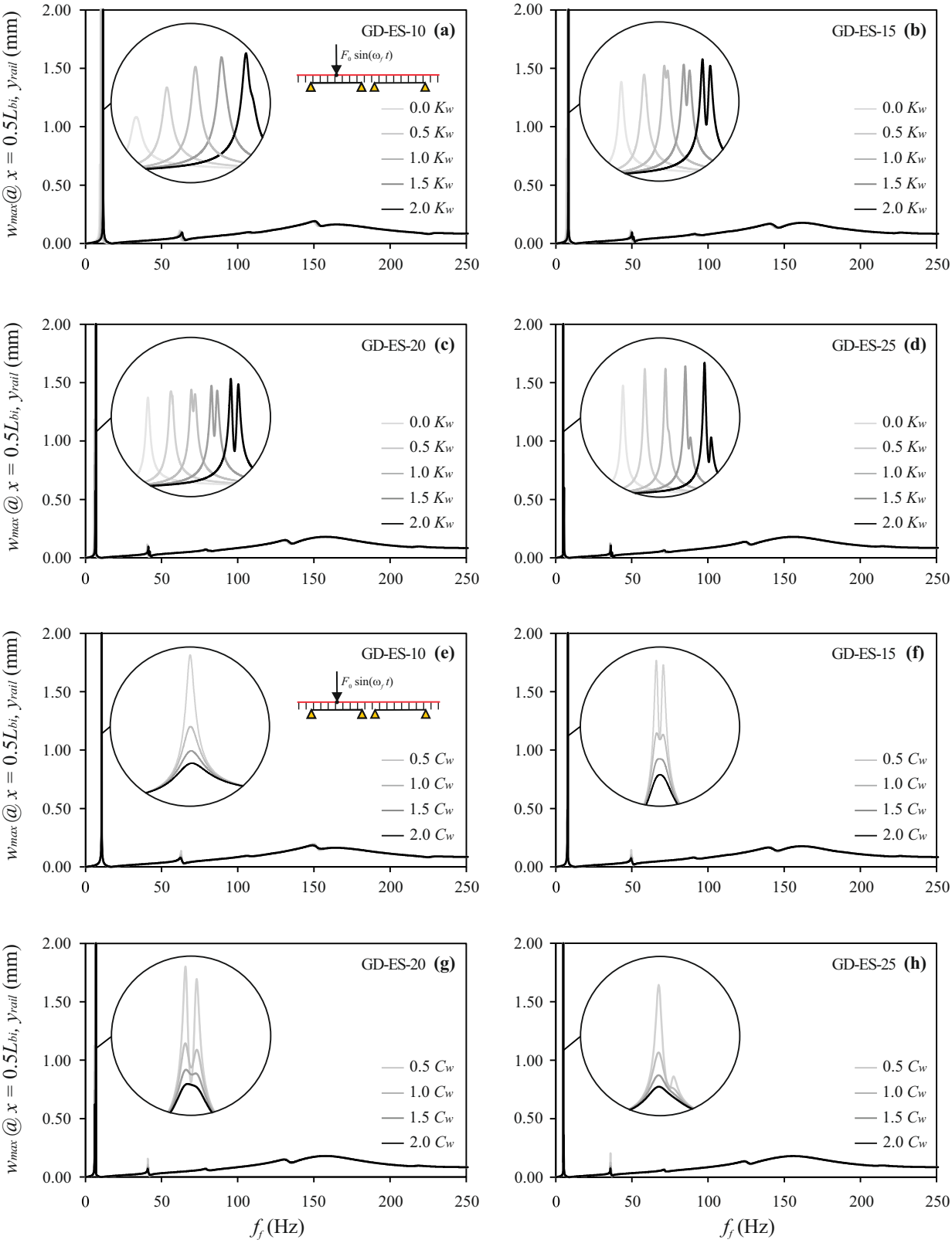

Figure 7: Harmonic analysis over the girder-deck elastically-supported bridges for individual variations of K_w and C_w.

The following is observed:

- A prominent narrow peak appears in the vicinity of the bridge fundamental frequency (see Table 1) corresponding to resonance of this mode. Due to the separation between the first and the second natural frequencies, for some lengths (L_{bi} = 15, 20 and 25 m), two peaks are perceptible instead of one. This relates to the slight variations in the number of sleepers between both spans, which makes the structure not perfectly symmetric. A wider maximum is also visible close to 150 Hz associated to modes with a high participation of the track. Smaller peaks appear along the curves with not-zero modal amplitude at mid-span of the first span.

- As K_w increases, so does the resonant frequency associated to the fundamental mode, consistently with the variations observed in the natural frequencies of the bridges (Fig. 6). The amplitude variation of this peak with K_w depends on the relative properties of the track and bridge systems.

- The response at resonance of the fundamental mode and of subsequent bridge modes at low frequencies reduces monotonically with C_w. The effect of this parameter at higher frequencies is negligible.

3.4. Influence of K_w and C_w on the maximum acceleration of the bridges under moving loads

In this section, the influence of K_w and C_w on the vertical response of the bridges under passing trains is investigated. To this aim, several dynamic analyses are carried out on the GD-ES-10 bridge under the circulation of the HSLM-A1 Universal Train presented in the EC. Only the results for this bridge are shown for the sake of conciseness and because it is the most influenced by the ballast shear stiffness and damping properties. The vertical acceleration is calculated with the aforementioned train in the speed range [40, 117] m/s (i.e. [144, 420] km/h) every 1 m/s at a quarter, mid-span and three quarters of both spans. A Chebyshev filter is applied to the response between 1 Hz and 60 Hz. Then, maximum response envelopes are obtained for each speed. The following individual variations of the track parameters are imposed: [0.0, 0.5, 1.0, 1.5, 2.0] $\times$ K_w and [0.5, 1.0, 1.5, 2.0] $\times$ C_w. Furthermore, Rayleigh damping is admitted according to EC for pre-stressed concrete bridges as 1.70% for the GD-ES-10 bridge. This ratio is applied on the first and fifth natural frequencies, being $f_1 = 10.61$ and $f_5 = 62.86$ Hz.

Figs. 8(a-b) show an envelope of the maximum acceleration in the most critical section of the bridge deck, which corresponds to the center of the second span. The maximum acceleration level is not relevant, as an unrealistically high design velocity is considered in order to capture low order and clear resonances of the bridge fundamental mode. Also, and in order to visualise how the variations of K_w and C_w affect the

bridge response in different situations, the acceleration time-history at the same section is represented for three different velocities.

In the first place, the second resonance speed of the first frequency mode (i.e. $j = 2$, $n = 1$) is calculated according to Eq. 3 as 345 km/h. In this expression, d stands for the characteristic distance of the HSLM-A1 train ($d = 18$ m), T_n is the n-th natural period of the bridge and j corresponds to the resonance order. The resulting time-histories presented in Figs. 8(c-d) show a clear second resonant response of the bridge leading to high amplification, especially for the lowest C_w value.

$$V_{nj}^{r} = \frac{d}{j\,T_n} = \frac{d\,\omega_n}{2\pi j} \tag{3}$$

The acceleration time-history is also calculated for a speed of 275 km/h (see Figs. 8(e-f)), which is far from resonance or from a theoretical condition of cancellation. Finally, the response is computed for a speed nearing cancellation of resonance (see Figs. 8(g-h)). Cancellation conditions are given in Eq. 4 and depend on the span length of the bridge and the characteristic distance of the train. Besides, λ_n stands for the root of the frequency equation of a beam with elastic supports at both ends, and K_{ni}^{c} is a parameter related to the phenomenon of cancellation, as indicated in reference [43]. In this sense, when the relation (L_{bi}/d) approaches the i-th cancellation ratio $(L_{bi}/d)_{nji}^{c}$, the annulment of resonance is produced and the vibration level gets significantly attenuated. For the GD-ES-10 bridge traversed by the HSLM-A1 train, the third resonance speed of the first mode, $V_{1,3}^{r} = 230$ km/h, approaches the first theoretical condition of cancellation ($(L_{bi}/d) = 0.56$ and $(L_{bi}/d)_{1,3,1}^{c} = 0.49$), although it is not coincident (the difference is approximately 12.5%). However, the phenomenon is visible, leading to a noticeable attenuation of the resonant peak.

$$\left(\frac{L_{bi}}{d}\right)_{nji}^{c} = \left(\frac{\lambda_n}{n\,\pi}\right)^{2} \frac{n}{2jK_{ni}^{c}}, \qquad n, j, i \geq 1 \tag{4}$$

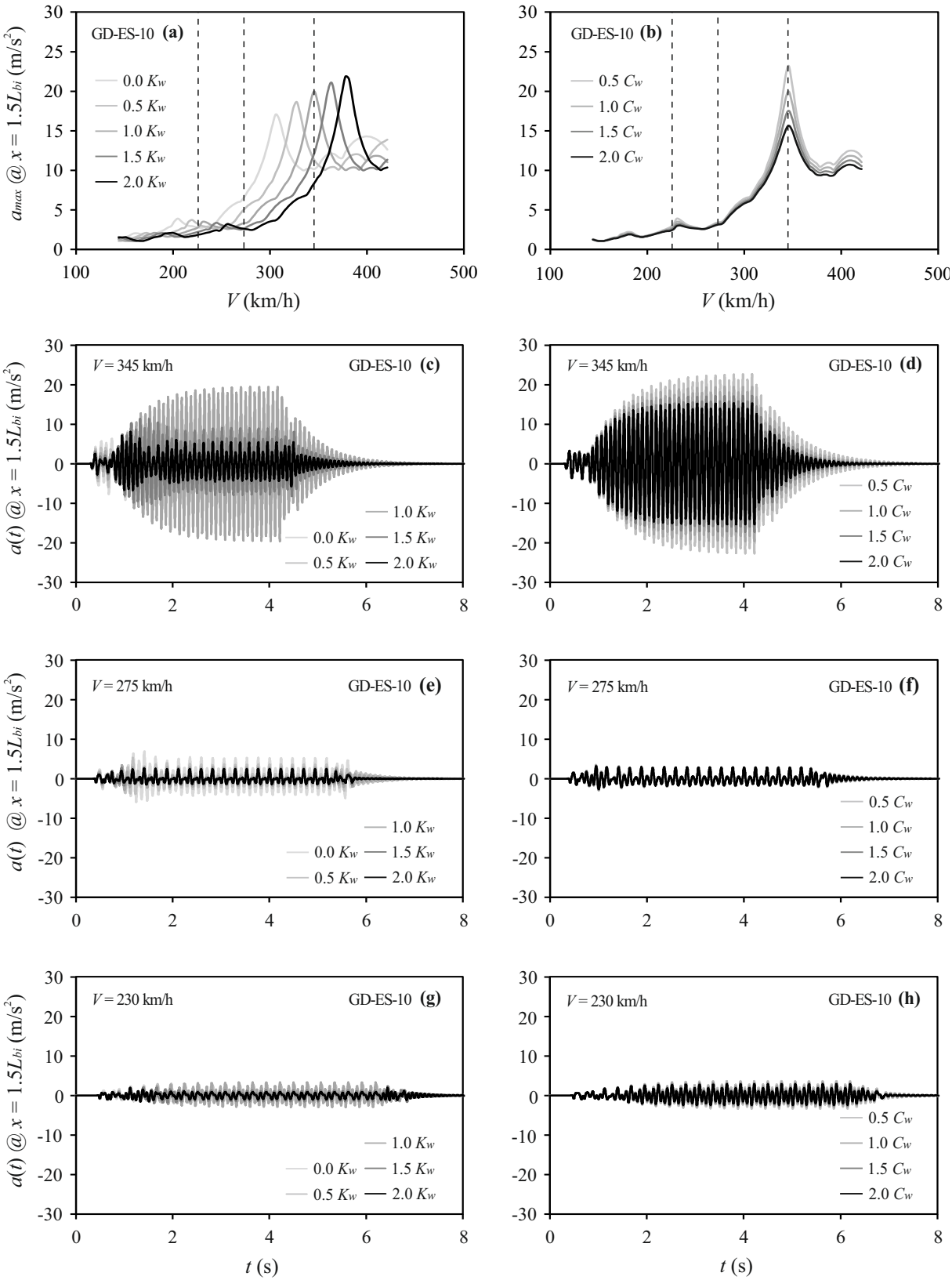

Figure 8: GD-ES-10 bridge: acceleration at $x = 1.5L$ under HSLM-A1 train. (a-b): a_{max} vs. V; (c-d): $a(t)$ near resonance (V = 345 km/h); (e-f): $a(t)$ for V = 275 km/h; (g-h): $a(t)$ near cancellation (V = 230 km/h).

In summary, the following observations can be made:

- As the ballast shear stiffness increases, so does the speed at which resonance takes place, in the same proportion as the natural frequency is altered by this parameter (in this particular case, neglecting or doubling K_w entails variations of -14.5% to +9.5% of the resonant velocity with respect to the nominal case). This affects similarly higher-order resonances.

- For the range of K_w values considered, resonance at a certain speed may or may not take place depending on the value of K_w (see Figs. 8(c-e)).

- Regarding the effect of the ballast shear damping, it is only relevant at resonance, leading to a pronounced reduction of the acceleration. In this particular case, if C_w doubles with respect to its nominal value, the vertical acceleration reduces by 25.5%. The effect of this parameter on the second resonant peak ($V^r_{1,2}$ = 345 km/h) is much higher than the effect on the third one ($V^r_{1,3}$ = 230 km/h). Nevertheless, this last peak is close to cancellation and no conclusions can be extracted in this regard.

- Finally, for the resonance speed approaching a cancellation condition, a notable attenuation of the acceleration level is observed with a small influence of the track parameters. As can be seen, cancellation of resonance takes place in the presence of the track despite the track parameters considered.

4. Weak coupling of the ballasted track between successive spans

4.1. Influence of the number of spans in the numerical models

A study on the effect of including an increasing number of identical structurally independent spans in the numerical models of the bridges is presented in this section. The maximum level of predicted acceleration and the section where it occurs may differ depending on the number of spans considered due to the vertical weak coupling exerted by the track in these structures. The results are included for both girder and slab bridges considering span lengths of L_{bi} = 10, 15, 20 and 25 m. The two versions of each bridge, considering (ES) and neglecting (SS) the vertical flexibility of the neoprene bearings, are investigated. The structures are analysed under the passage of a particular train in the speed range [40, 117] m/s in 1 m/s steps (see Table 4). As shown below, a different Universal Train is selected for each bridge in order to obtain a clear resonant response and avoid cancellation of resonance conditions. Then, the maximum acceleration and displacement responses are computed at nine sections per span with a 0.1 $\times$ L_{bi} spacing. Envelopes of maximum response are obtained considering single-span, two-span and three-span models for each bridge.

Bridge	Train	d [m]
GD-ES/SS-10	HSLM-A1	18
GD-ES/SS-15	HSLM-A6	23
GD-ES/SS-20	HSLM-A4	21
GD-ES/SS-25	HSLM-A9	26
SD-ES/SS-10	HSLM-A3	20
SD-ES/SS-15	HSLM-A10	27
SD-ES/SS-20	HSLM-A4	21
SD-ES/SS-25	HSLM-A5	22

Table 4: Passing trains and corresponding characteristic distances d selected for the girder and slab bridges.

The results are shown in Fig. 9 for the girder bridges, and in Fig. 10 for the slab bridges. In both graphs, the amplification ratio $\overline{a}_{max}(x)$ is represented to compare the results of the three models. This parameter represents the quotient between the maximum acceleration predicted in the complete range of velocities at a particular section x of the bridge with the two or the three-span models ($a_{max}(x)$) and the overall maximum acceleration predicted by the single-span model $a_{max}^{N_{sp}=1}$. A similar amplification ratio $\overline{d}_{max}(x)$ is defined for the displacement.

$$\overline{a}_{max}(x) = \frac{a_{max}(x)}{a_{max}^{N_{sp}=1}} \qquad \overline{d}_{max}(x) = \frac{d_{max}(x)}{d_{max}^{N_{sp}=1}} \tag{5}$$

In both figures, solid gray columns represent the acceleration amplification $\overline{a}_{max}(x)$: dark grey indicates ES bridges and light grey SS ones. Over these columns, the displacement amplification $\overline{d}_{max}(x)$ is represented using hollow black-contours. Notice that values standing above the dashed line indicate that the response predicted by the two or the three-span model exceeds the maximum overall response predicted by the single-span model.

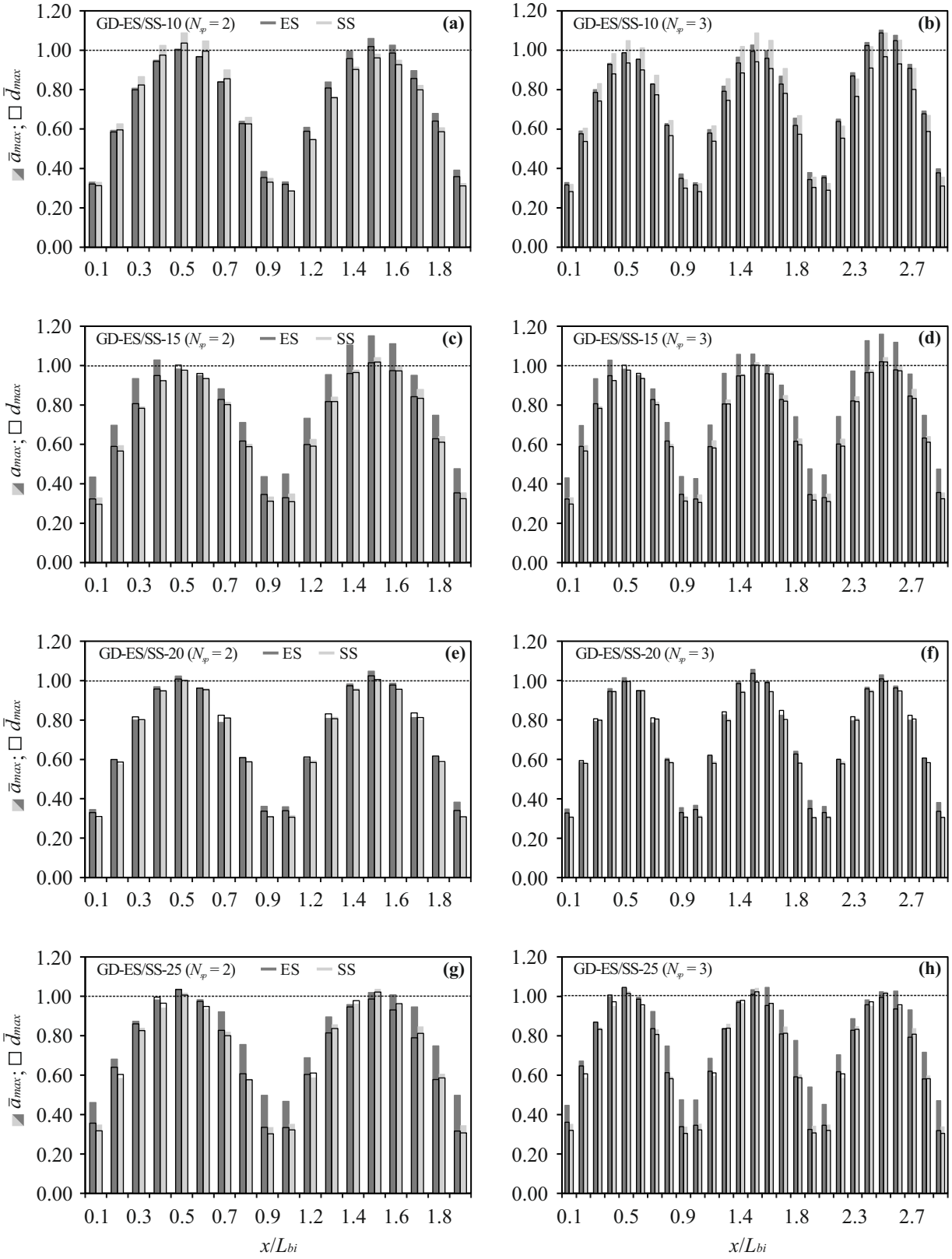

Figure 9: Girder bridges: amplification acceleration $\overline{a}_{max}(x)$ and displacement $\overline{d}_{max}(x)$ ratios at each bridge x coordinate considering models with two spans (left) and three spans (right).

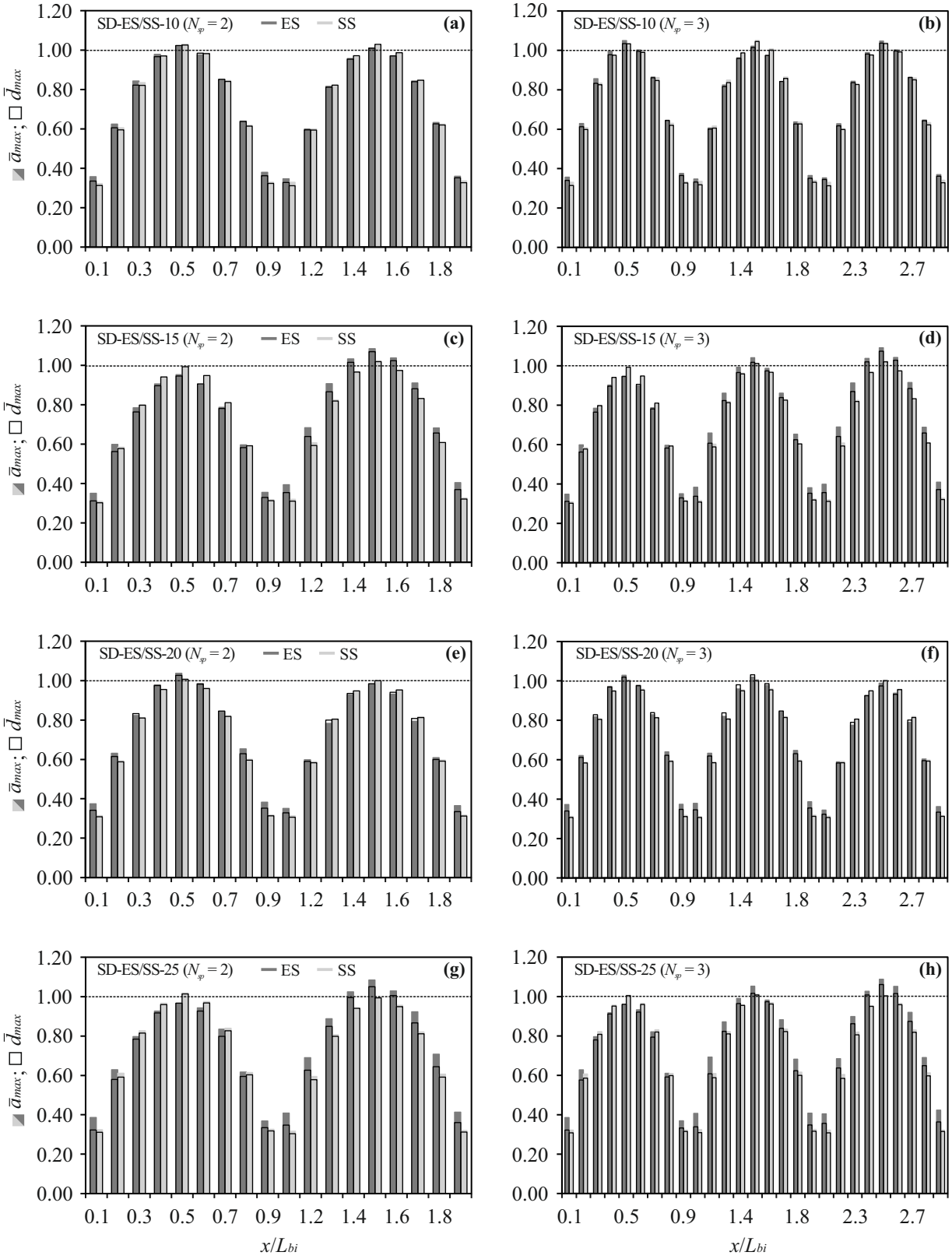

Figure 10: Slab bridges: amplification acceleration $\overline{a}_{max}(x)$ and displacement $\overline{d}_{max}(x)$ ratios at each bridge x coordinate considering models with two spans (left) and three spans (right).

From the results obtained, the following remarks can be made:

- In all the cases, maximum acceleration and displacement responses predicted with the single-span model occur at mid-span. However, when more than one span is considered, the maximum response does not necessarily take place in the center of the first span.

- For the girder bridges, when $N_{sp} = 2$, the maximum response takes place at the center of the second span when neoprenes are included (ES case) and when $L_{bi} = 10$, 15 and 20 m. Peak deviations of +15% and +1%, in terms of acceleration and displacement ($\overline{a}_{max}(x) = 1.15$ and $\overline{d}_{max}(x) = 1.01$), respectively, are achieved for the GD-ES-15 bridge. This implies that the two-span model predicts a higher response than the single-span model. In the SS case, except for the $L_{bi} = 10$ m case, the differences are negligible. When $N_{sp} = 3$, the maximum response occurs at the center of the third span in the two shortest bridges: $L_{bi} = 10$ and 15 m. This is especially clear for the ES case, although it also happens to a lower extent in the SS case. The highest disparities are found in the GD-ES-15 bridge, reaching +16% and +2% with respect to the predictions of the single-span model in terms of acceleration and displacement, respectively. For the longest bridges ($L_{bi} = 20$ and 25 m), the response is also higher than that calculated with the single-span model. However, the differences are not relevant in these cases.

- For the slab bridges, when $N_{sp} = 2$, the maximum response occurs at the center of the second span when $L_{bi} = 15$ and 25 m in the ES case. Higher divergences are found in the SD-ES-15 bridge, reaching +8% for acceleration and +7% for displacement, in comparison to the single-span model predictions. For the SS case, differences are negligible. When $N_{sp} = 3$, the maximum response occurs at the center of the third span for $L_{bi} = 10$, 15 and 25 m in the ES case. The highest deviation is found in the SD-ES-15 bridge with +9% and +7% higher levels of acceleration and displacement, respectively. For the SS case, even if the predicted response may be greater with the three-span model, the divergences with respect to the single-span model are not relevant.

Finally, in Figure 11 maximum acceleration envelopes are represented to show the origin of the differences detected in the previous analyses. For the sake of conciseness, only resonance curves for the $L_{bi} = 15$ m girder and slab deck bridges are provided, as the differences with respect to the one-span model are more evident in this case. The maximum acceleration at the most critical section of the bridge is represented versus the nondimensional speed $V/f_1 d$ of the corresponding HSLM-A trains for the one and three-span bridges. Resonances of the same order appear aligned vertically. Notice that $V/f_1 d = j^{-1}$, for j being the

resonance order. In both GD-ES/SS-15 and SD-ES/SS-15 bridges, the acceleration at the second resonance, which causes the maximum response, predicted with the three-span model is higher than that predicted with the single-span model. This amplification in the response is higher in the girder bridges and in the ES case.

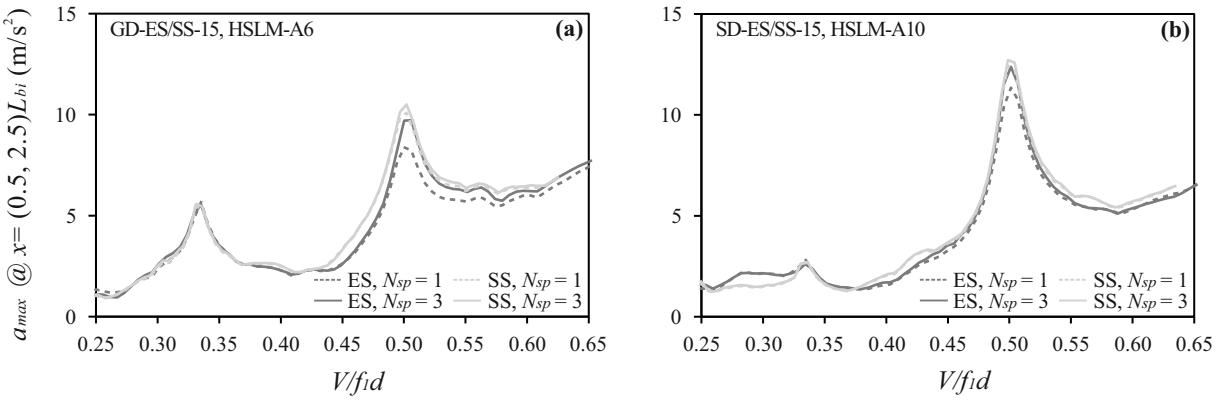

Figure 11: Resonance curves of the (a) GD-ES/SS-15 and (b) SD-ES/SS-15 bridges.

5. Case study: numerical-experimental comparison on a real bridge

5.1. Old Guadiana Bridge description and model calibration

In what follows, the response of an existing railway bridge under operating conditions is reproduced numerically and compared to experimental measurements. A short girder bridge with moderate flexural stiffness is selected as these bridges have proven to be the most affected by the ballast shear effects. The structure is located in a non-seismic zone in the conventional railway line Madrid - Cádiz, in the Alcázar de San Juan - Manzanares section. It crosses the Old Guadiana watercourse (see Fig. 12) with two identical SS spans of 11.93 m each. The structure is a double-track bridge composed by two structurally independent adjacent decks (one for each ballasted track). The decks consist of a reinforced concrete slab on top of five pre-stressed concrete rectangular girders (see Fig. 13) which rest on two abutments and on a central support by means of laminated neoprene bearings. The tracks present Iberian gauge with UIC 60 rails and mono-block concrete sleepers every 0.60 m.

The authors performed an experimental campaign on the bridge in May 2019, with the aim to determine the modal parameters and the dynamic response of the structure under operating conditions. 18 accelerometers were installed underneath the girders according to the layout shown in Fig. 14. The dynamic response

Figure 12: Bridge over the Old Guadiana watercourse images.

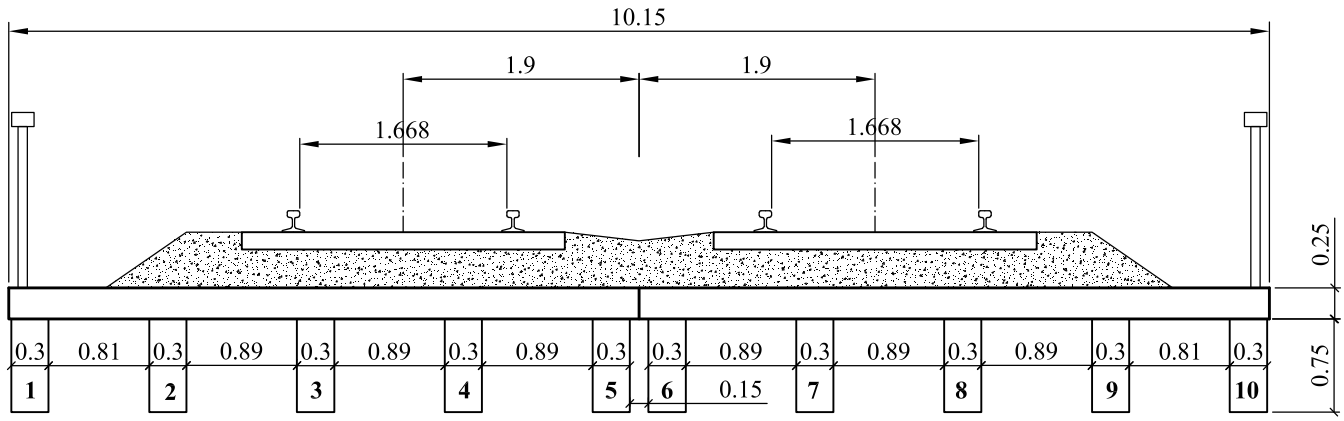

Figure 13: Old Guadiana bridge cross-section.

of the bridge was measured under ambient vibration to identify the modal parameters. Also, the vertical acceleration of the structure was recorded under the passage of several trains, and, additionally, modal damping ratios were identified from the free vibrations left by them. For additional information about this campaign the reader is referred to reference [15]. The fundamental mode of the structure corresponds to the first longitudinal bending mode of both decks vibrating in phase. Subsequent modes below 30 Hz are related to the torsional and transverse bending deformation of the structure. Table 5 contains the natural frequencies (f_{exp}) and the damping ratios (ζ_{exp}) identified experimentally for the first five modes.

Mode	1	2	3	4	5
f_{exp} [Hz]	9.84	11.03	12.84	21.43	28.74
ζ_{exp} [%]	2.8	2.6	1.5	1.5	1.0

Table 5: First five natural frequencies and the corresponding damping ratios identified experimentally.

The numerical model of the bridge described in section 2 is calibrated by means of an optimisation iterative procedure based on a Genetic Algorithm (GA) [44] implemented in MATLAB v.2017b and ANSYS v.17.1.0. In the updating process, an objective function involving the numerical-experimental difference of

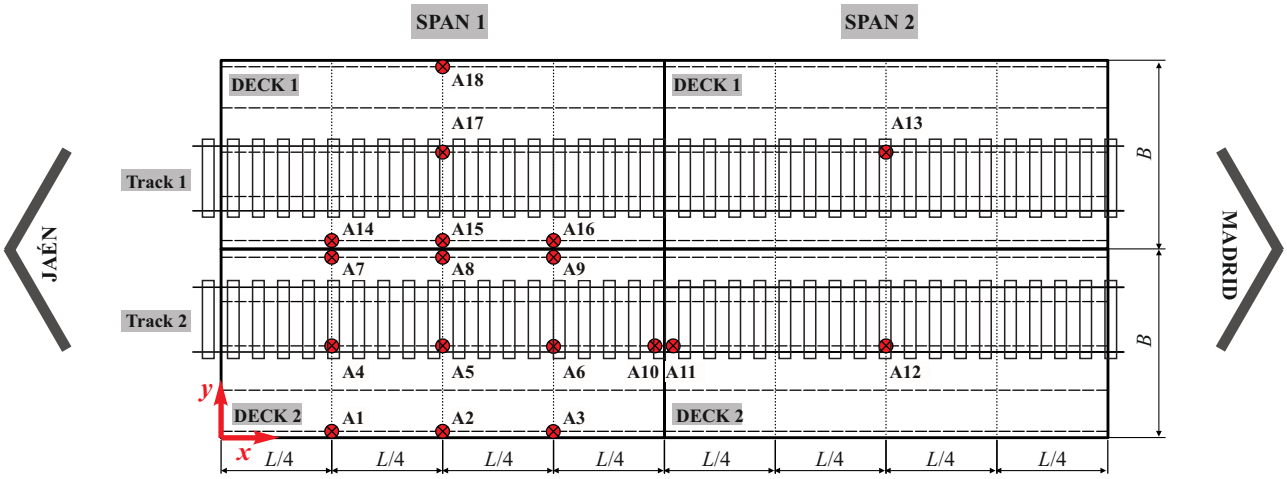

Figure 14: Sensors layout in Old Guadiana bridge.

the fundamental frequencies, the MAC residuals and the static displacement at mid-span during a proof-load test is minimised. The data for this last comparison are extracted from [45].

$$F_{obj}(P) = \left| \frac{f_{1\,exp} - f_{1\,num}(P)}{f_{1\,exp}} \right| + (1 - \mathrm{MAC}_1(P)) + \left| \frac{\delta_{exp} - \delta_{num}(P)}{\delta_{exp}} \right| \tag{6a}$$

$$P = (E_{bi}I_{bi}, m_{bi}, K_w, R) \tag{6b}$$

Four parameters are selected for calibration (Eq. 6b) on the basis of preliminary sensitivity tests and of the level of knowledge and certainty on the track-bridge system properties. These correspond to the bridge bending stiffness $E_{bi}I_{ybi}$, the linear mass of the deck m_{bi}, the ballast shear stiffness K_w and the neoprene dynamic coefficient R, defined by Eq. 7.

$$R = \frac{\bar{K}^n_{bi,dyn}}{\bar{K}^n_{bi,st}} \tag{7}$$

Both spans are considered identical. Initial values and optimisation ranges are chosen on the basis of engineering considerations and from applicable data from previous publications. For $E_{bi}I_{ybi}$ and m_{bi}, the initial values are calculated from the structural description and technical drawings in [45]. As the information about K_w in the literature is scarce, the reference value $K_w = 7.84 \times 10^7$ N/m from Table 3 is selected as initial guess and a wide range of variation for this parameter is admitted. In relation to R, the initial value is set to 2, as commonly admitted for dynamic loads. The range of variation is selected between this

same value and 1.10, as indicated in [46]. The static vertical stiffness of the neoprene bearings is set to $\bar{K}^n_{bi,st} = 5.5825 \times 10^8$ N/m from a pre-design based on the bridge available information. The rest of the parameters of the model are those listed in Table 3. Rayleigh damping is admitted as 1.56% for the first and fifth frequency modes on the basis of EC.

The updated values for the four parameters are included in Table 6. This table shows the results after running the GA several times to ensure the stability of the solution and the updating procedure. A population size of 40 (10 times the number of calibration parameters) and 200 generations are considered. Mutation and crossover rates are set to 0.02 and 0.8, respectively, while the probability of tournament is set to 0.7 and the scale of mutation to 0.1. The final variation of the parameters is well contained in the calibration ranges, obtaining a satisfactory optimised solution.

Notation	Parameter	Initial value	Optimisation range	Final value	Unit
$E_{bi}I_{ybi}$	Bridge bending stiffness	7086.760	$[-20, +20]\%$	7012.859	MNm^2
ρA	Bridge linear mass	7031.411	$[-5, +5]\%$	7002.779	kg/m
K_w	Ballast shear stiffness	7.840×10^7	$[-40, +40]\%$	9.271×10^7	N/m
R	Neoprene dynamic coefficent	2.0	$[1.1, 2.0]$	1.652	–

Table 6: Model initial and updated parameters.

Table 7 shows the performance of the updated solution provided by the GA. The experimental and numerical values for the fundamental frequency of the bridge are expressed as f_{1exp} and f_{1num}, respectively, while e_{f100} stands for the fundamental frequency difference (first term in Eq. 6a) as a percentage. The next columns indicate the maximum experimental (δ_{exp}) and numerical (δ_{num}) deflection at the center of the first span during the proof-load test, and also the corresponding difference, $e_{\delta 100}$ (last term in Eq. 6b) as a percentage. Finally, the last column shows the MAC for the fundamental mode. The low differences and the MAC number indicate that a good agreement is achieved with the updating procedure in terms of modal parameters and static deflection.

Parameter	f_{1exp} [Hz]	f_{1num} [Hz]	e_{f100}[%]	δ_{exp} [mm]	δ_{num} [mm]	$e_{\delta 100}$[%]	MAC_1 [–]
Updated solution	9.8400	9.8406	0.0061	-1.9055	-1.9053	0.0094	0.9871

Table 7: Experimental and numerical values for the fundamental frequency, static deflection and MAC number after calibration.

5.2. Acceleration response under train passages

The passages considered for the analysis are those corresponding to the commercial RENFE medium distance trains S449 and Altaria Talgo. Table 8 includes the track number and travelling direction (J: Jaén, M: Madrid), coaches configuration (L: locomotive, C: carriage), circulating speed and axles scheme

and load values. S449 is an articulated train with distributed power, composed of two integrated driver-passenger cars at both ends and three passenger coaches in between. The distance between shared bogies is $d = 17.75\,\text{m}$. Altaria Talgo is a regular train made up of a Talgo 252 locomotive and 9 passenger coaches with a characteristic distance $d = 13.14\,\text{m}$.

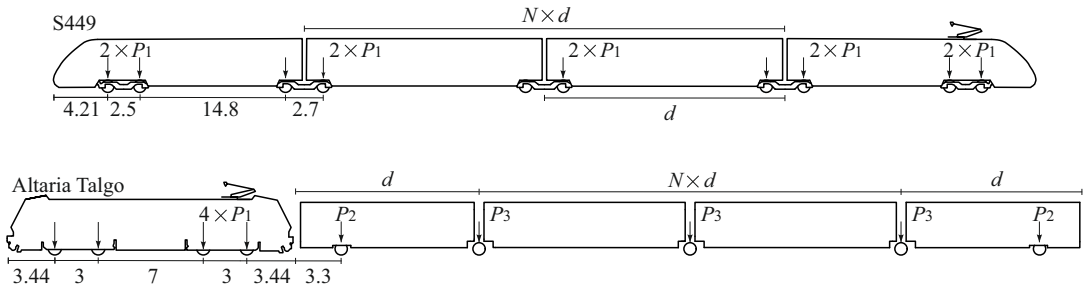

Train	Track	Ride	Scheme	V [km/h]	N	d [m]	P_1 [kN]	P_2[kN]	P_3[kN]
S449	2	J-M	L-3C-L	160.2	3	17.75	161	–	–
Altaria Talgo	1	M-J	L-9C	154.8	7	13.14	225	70	140

Table 8: RENFE S449 and Altaria Talgo passages information.

The experimental response is extracted from the sensors located at the center of each span in the direction of motion: A5 (first span) and A12 (second span) for the S449, which circulated heading to Madrid along track 2; and A13 (first span) and A17 (second span) for the Altaria Talgo, which circulated in the opposite direction along track 1 (see Fig. 14). Both the numerical and the experimental responses are filtered applying two Chebyshev filters with high-pass and low-pass frequencies of 1 Hz and 30 Hz, respectively. To appropriately reproduce the dynamic response of the bridge, an additional calibration step is performed for the ballast shear damping C_w, using the Frequency Amplitude Assurance Criterion (FAAC) and the Frequency Response Assurance Criterion (FRAC) [47, 48]. These correlation criteria are evaluated at a particular sensor i according to Eq. 8a and Eq. 8b, respectively, where $H(\omega)^{exp}$ corresponds to the value of the experimental Frequency Response Function (FRF) at a certain frequency ω and $H(\omega)^{num}$ to its numerically predicted equivalent. The superscript H stands for the Hermitian conjugate of the corresponding matrices. FAAC and FRAC criteria are sensitive to inconsistencies in the amplitude and in the shape of the FRFs, respectively. They both work in the frequency domain and return a real number in the range [0, 1], where unity indicates perfect correlation.

$$FAAC_i = \frac{2|(H_i^{exp}(\omega))^H H_i^{num}(\omega)|}{((H_i^{exp}(\omega))^H H_i^{exp}(\omega)) + ((H_i^{num}(\omega))^H H_i^{num}(\omega))} \tag{8a}$$

$$FRAC_i = \frac{|(H_i^{exp}(\omega))^H H_i^{num}(\omega)|^2}{((H_i^{exp}(\omega))^H H_i^{exp}(\omega))\,(H_i^{num}(\omega))^H H_i^{num}(\omega))} \tag{8b}$$

Based on these criteria, a preliminary analysis is performed with the updated model while applying variations for the ballast shear damping. Fig. 15 shows the computed values for FAAC and FRAC numbers as a function of C_w at the center of each span of the bridge. As can be seen, FAAC values are higher than FRAC ones. This is understandable, as the planar characteristics of the numerical model and the moving load train representation may impede a very accurate prediction of the whole complexity of the FRF shape. Also, the proximity of the actual velocity of the Altaria Talgo train to a third theoretical resonance speed $V_{1,3}^r = 154$ km/h may explain to some extent the divergence level in the FAAC and FRAC numbers. In any case, an updated value of $C_w = 6.00 \times 10^5$ Ns/m is selected based on the progression of both parameters under operating conditions, as at that point, the average difference between previous values for the FAAC and FRAC numbers falls under 10%. The corresponding values for these parameters are listed in Table 9.

Train	FAAC 1^{st} span	FRAC 1^{st} span	FAAC 2^{nd} span	FRAC 2^{nd} span
S449	0.66	0.57	0.74	0.56
Altaria Talgo	0.68	0.50	0.66	0.45

Table 9: FAAC and FRAC criteria applied to sensors A5 and A12 for the S449 train and A13 and A17 for the Altaria Talgo train for $C_w = 6.00 \times 10^5$ Ns/m.

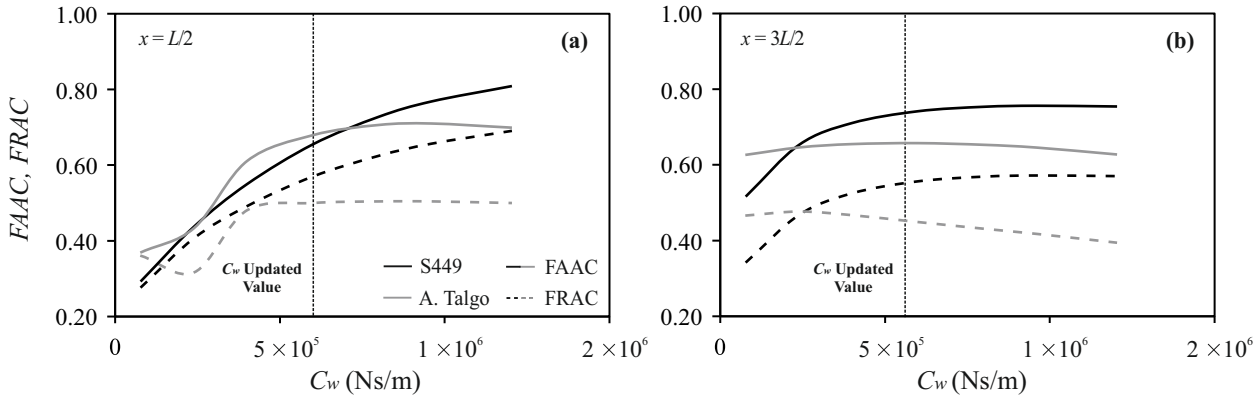

Figure 15: FAAC and FRAC coefficients as a function of C_w, which is expressed per rail seat.

Finally, the vertical response of the bridge under the passage of the S449 and Altaria Talgo trains

is computed and compared with the experimental data at the center of each span in Figs. 16 and 17, respectively. In both figures, the vertical acceleration is represented in the time domain (a-b) and in the frequency domain (c-d). The gray line represents the experimental data and the black one the numerical response. From the results shown in these figures, the following is concluded:

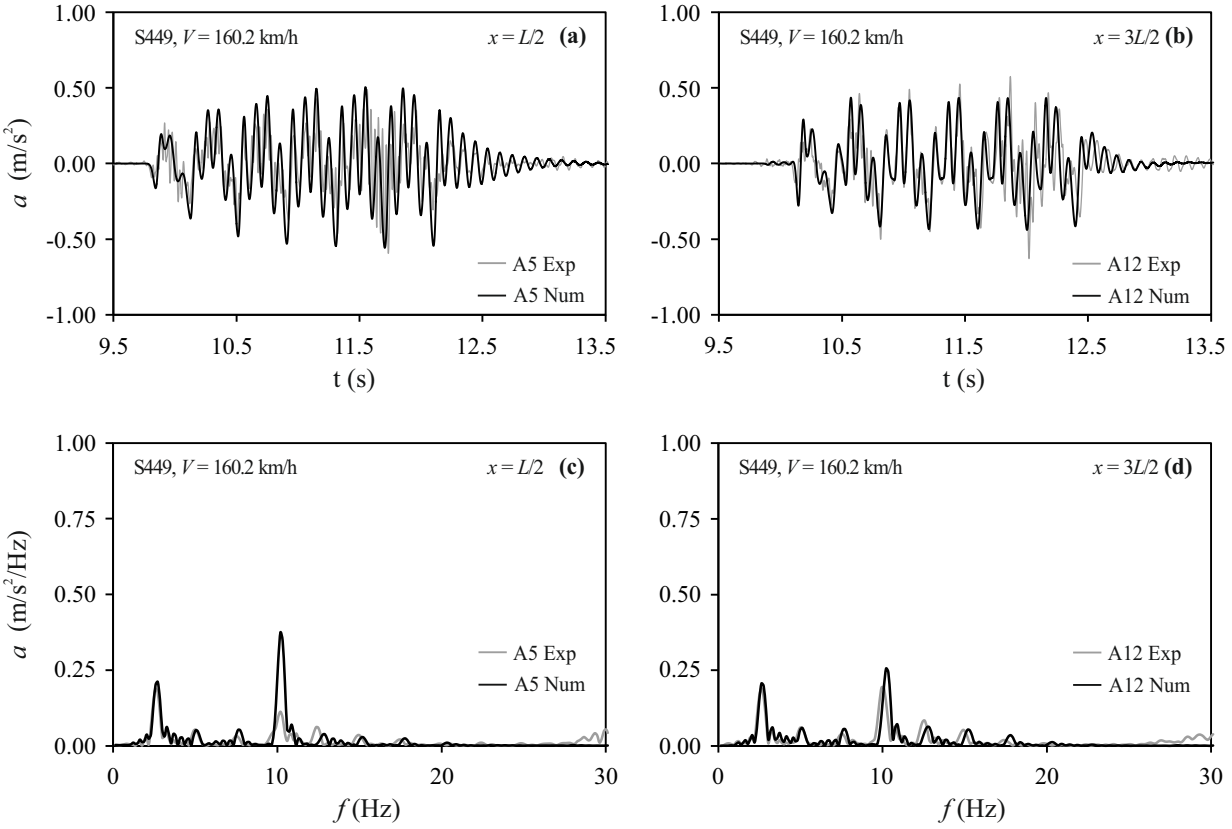

Figure 16: Train S449: Time history (a-b) and frequency content of the acceleration (c-d) at the center of each span.

- The 2D planar track-bridge interaction model and the calibration strategy seem correct as, in general, the experimental response is adequately reproduced in the frequency range of interest. The integration of the dynamic equations using the full FE model, and the consideration of distributed damping along the track, lead to a better numerical-experimental matching when compared to applying Modal Superposition and using modal damping coefficients.

- The response is adequately reproduced both in the time and frequency domains, with an even better adjustment in the second span in the traveling direction. The numerical model overpredicts the response close to the fundamental frequency of the bridge. It is highly probable that the reason for

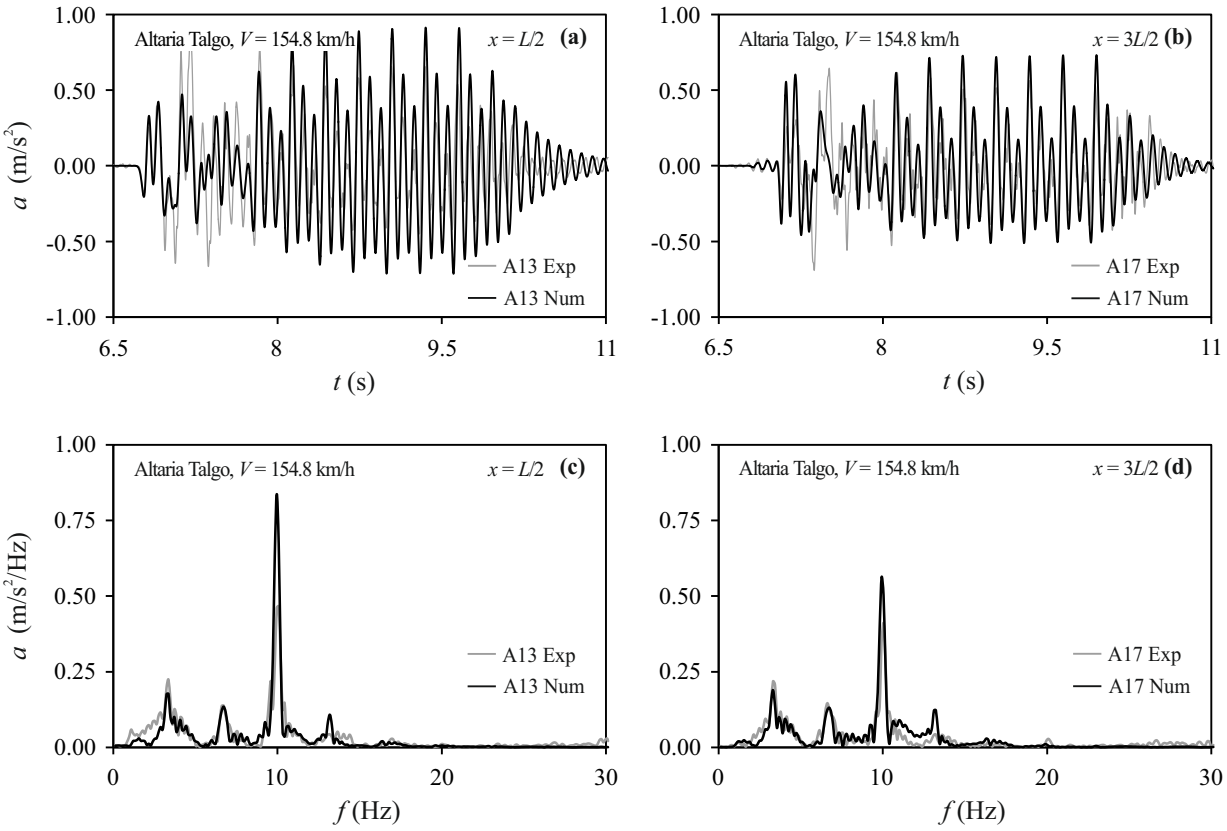

Figure 17: Train Altaria Talgo: Time history (a-b) and frequency content of the acceleration (c-d) at the center of each span.

this discrepancy is caused by the fact that VBI is not included in the model. The train suspension systems interact with the bridge vibrations and absorb part of the energy, altering the structural response, especially when resonance occurs and when the interaction between both systems is relevant ([49],[21]). This is more important in the Altaria Talgo case, because of the proximity of the circulating velocity to a theoretical third resonance. However, in general, both curves have a good resemblance.

- Given the relevance of the track parameters in the bridge model updating and dynamic response, especially as far as ballast shear mechanisms are concerned, reliable values for these properties to be used in discrete track-bridge interaction models should be obtained for different track characteristics and states of conservation, based on experimental studies.

6. Conclusions

This contribution provides a detailed sensitivity analysis about the influence of the ballasted track on the dynamic response of single-track railway bridges of different characteristics. For this purpose, a planar track-bridge interaction model is employed. In the first place, the effect caused by ballast shear mechanisms, represented through the discrete stiffness and damping parameters K_w and C_w, is studied on the modal parameters, on the harmonic response and on the vertical acceleration of the bridges under train passages. Then, the effect of the weak coupling exerted by the continuity of the ballasted track is evaluated through a series of analyses in order to assess the necessity of including more than one span in the discrete numerical models of multi-span SS bridges. Finally, the numerical model is updated applying an iterative procedure based on a Genetic Algorithm with experimental data from an existing bridge and an experimental-numerical comparison is presented under operating conditions.

The main conclusions derived regarding the influence of the main track parameters on the dynamic response of the bridges are:

- When using discrete track-bridge interaction models as the one presented, K_w and C_w are the parameters that affect the most the bridge dynamic response in the frequency range of interest. The remaining parameters have a negligible influence compared to these two.

- K_w exerts a notable influence on the modal parameters of the bridges, which is stronger in shorter structures. With respect to the typology, girder-deck bridges are the most affected due to their initially lower bending stiffness. The correlation of this effect with the flexibility of the elastic supports is minor.

- The influence of K_w and C_w on the harmonic response is relevant only at low frequencies. An increase in K_w causes a rise in the fundamental frequency of the bridges. Its influence is less relevant on higher modes. The increment of C_w provokes a pronounced reduction of the corresponding amplitude, as could be expected. Higher frequencies related to track deformation modes are not especially affected by these parameters.

- The effect of K_w and C_w on the vertical acceleration response of the bridges under passing trains is important, especially at resonance. An increment of K_w leads to a raise in the resonance speeds, proportional to the variation of the bridge natural frequencies, while an increment of C_w results into a reduction of the resonant a amplitude. However, the influence of C_w far from resonance is negligible. Furthermore, the cancellation phenomenon still occurs when the track is included regardless of the

track properties. Therefore, in general terms the consideration of the ballast shear transfer mechanisms could be beneficial for the assessment of the dynamic performance of short span bridges located in railway lines in which an increase of the maximum circulating speed is envisaged, since the critical circulating speeds leading to inadmissible acceleration levels might exceed the maximum design speed and the resonant acceleration levels could be lower due to the additional damping associated to the ballast track-bridge interaction.

With respect to the analysis involving the weak coupling of the track in numerical models of multi-span bridges, it is concluded that:

- Discrete track-bridge simplified single-span models may not predict the maximum response in multi-span structures due to the effect caused by the weak coupling of the track, and, therefore, they may not be on the safe side. Plus, the maximum response may not take place in the center of the first span. This is especially clear in the case of shorter girder bridges when the neoprene bearings are included.

As for the numerical-experimental comparison included in the case study:

- The numerical results have an agreeable concordance with the experimental data. Discrete track-bridge interaction models can be an adequate solution that allows us to solve the dynamic equations of motion in the time domain performing a full analysis in a reasonable amount of time, which can be useful for conceptualization, design and decision-making purposes in engineering and technical consultancies.

This investigation addresses the gaps and explores the complexity of the train induced vibration phenomenon, which is a key aspect in order to develop a better and safer railway infrastructure. In this study, general conclusions are derived from a multi-level analysis carried out on a comprehensive bridge catalogue of different lengths and typologies. However, future investigations are required to fully understand the effect of the ballasted track on the dynamic behaviour of railway bridges involving more complex analyses. It is required to fully understand the influence of the ballast shear parameters and to find clear ways to quantify them, since their influence on the bridge dynamics is relevant and the information about it found in the literature is scarce. Reliable values for these parameters to be used in discrete track-bridge interaction models should be obtained for different track characteristics and states of conservation, based on experimental studies.

Acknowledgements

The authors would like to acknowledge the financial support provided by the Junta de Andalucía and the European Social Fund through the contract USE-22311-R with the Universidad de Sevilla, and also the Spanish Ministry of Science and Innovation under research project PID2019-109622RB-C2 and Generalitat Valenciana under research project AICO/2021/200.

References

[1] European Comission. Communication from the comission concerning the development of a Single European Railway Area, Technical report, 2010.

[2] Y., Clemente, (January 6th, 2019). La red ferroviaria en España. El País. Recovered from elpais.com.

[3] L. Frýba, Dynamic behaviour of bridges due to high-speed trains, in: Workshop for high-speed railways, in: Bridges for High-Speed railways, CR Press, 2008, pp. 137–158.

[4] CEN/TC250, EN 1990. Eurocode: Basis of structural design. Annex A2: Application for bridges. Final version, European Committee for Standardization, Brussels, 2005.

[5] CEN, EN 1991-2, Eurocode 1: Actions on Structures - Part 2: Traffic loads on bridges, European Committee for Standardization, Brussels, 2003.

[6] M. Zacher, M. Baeβler, Dynamic behaviour of ballast on railway bridges, in: Taylor&Francis (Ed.), Dynamics of High-Speed Railway Bridges, no. 978-0-203-89540-5, 2008, pp. 99–112.

[7] W. Hoorpah, Dynamic calculations of high-speed railway bridges in France: some case studies, in: Dynamics of High-Speed Railway Bridges, 2008.

[8] J. M. Rocha, A. A. Henriques, R. Calçada, Probabilistic safety assessment of a short span high-speed railway bridge, Engineering Structures 71 (2014) 99–111.

[9] C. Rebelo, L. Silva, C. Rigueiro, M. Pircher, Dynamic behaviour of twin single-span ballasted railway viaducts. field measurements and modal identification, Engineering Structures 30 (2008) 2460–2469.

[10] L. Bornet, A. Andersson, J. Zwolski, J. Battini, Influence of the ballasted track on the dynamic properties of a truss railway bridge, Structure and Infrastructure Engineering 11 (6) (2015) 796–803.

[11] K. Liu, E. Reyneders, G. D. Roeck, G. Lombaert, Experimental and numerical analysis of a composite bridge for high-speed trains, Journal of Sound and Vibration 320 (2009) 201–220.

[12] G. Chellini, L. Nardini, W. Salvatore, Dynamical identification and modelling of steel-concrete composite high-speed railway bridges, Structure and Infrastructure Engineering 7 (11) (2011) 823–841.

[13] K. Liu, G. Lombaert, G. D. Roeck, Dynamic analysis of multispan viaducts with weak coupling between adjacent spans, Journal of Bridge Engineering 19 (1) (2014) 83–90.

[14] K. Matsuoka, A. Collina, C. Somaschini, M. Sogabe, Influence of local deck vibrations on the evaluation of the maximum acceleration of a steel-concrete composite bridge for a high-speed railway, Engineering Structures 200 (2019) 109736.

[15] P. Galvín, A. Romero, E. Moliner, G. De Roeck, M. Martínez-Rodrigo, On the dynamic characterisation of railway bridges through experimental testing, Engineering Structures 226 (2020) 111261.

[16] E. Moliner, M. Martínez-Rodrigo, P. Galvín, J. Chordà-Monsonís, A. Romero, On the vertical coupling effect of ballasted tracks in multi-span simply-supported railway bridges under operating conditions, Structure and Infrastructure Engineering (2022) 1–23.

[17] M. Martínez-Rodrigo, E. Moliner, A. Romero, P. Galvín, Maximum resonance and cancellation phenomena in orthotropic plates traversed by moving loads: Application to railway bridges, International Journal of Mechanical Sciences 169 (2020) 105316.

[18] W. Zhai, K. Wang, J. Lin, Modelling and experiment of railway ballast vibrations, Journal of Sound and Vibration 270 (2004) 673–683.

[19] S. Monleón-Cremades, Cuadernos de Concepción de Puentes, Marco general, equipamientos y diseño de estructuras, 2002.

[20] Ministerio de Fomento. Gobierno de España, Instrucción de acciones a considerar en puentes de ferrocarril (2010).

[21] A. Doménech, P. Museros, M. Martínez-Rodrigo, Influence of the vehicle model on the prediction of the maximum bending response of simply-supported bridges under high-speed railwaytraffic, Engineering Structures 72 (2014) 123–139.

[22] T. Arvidsson, R. Karoumi, Train–bridge interaction – a review and discussion of key model parameters, International Journal of Rail Transportation 2 (3) (2014) 147–186.

[23] D. Ahlbeck, H. Meacham, R. Prause, The development of analytical models for railroad track dynamics, in: A. Kerr (Ed.), Railroad track mechanics & technology, Pergamon Press, 1978.

[24] P. Lou, A vehicle-track bridge interaction element considering vehicle's pitching effect, Finite Elements in Analysis and Design 41 (2005) 397–427.

[25] R. Clark, P. Dean, J. Elkins, S. Newton, An invesigation into the dynamic effects of railway vehicles running on corrugated rails, Journal of Mechanical Engineering Science 24 (2) (1982) 65–76.

[26] Q. Wu, Y. Sun, M. Spiryagin, C. Cole, Railway track longitudinal force model, Vehicle System Dynamics 59 (1) (2021) 155–170.

[27] Y. Ji, Y. J. Kim, State-of-the-art review of bridges under rail transit loading, Proceedings of the Institution of Civil Engineers - Structures and Buildings 172 (6) (2019) 451–466.

[28] J. Luo, S. Zhu, Z. W., An advanced train-slab track spatially coupled dynamics model: Theoretical methodologies and numerical applications, Journal of Sound and Vibration 501 (2021) 116059.

[29] B. Pring, A. Ruiz-Teran, Modelling traffic action in high-speed railway bridges, Proceedings of the Institution of Civil Engineers - Bridge Engineering 173 (3) (2019) 123–142.

[30] J. Sánchez-Quesada, E. Moliner, A. Romero, P. Galvín, M. Martínez-Rodrigo, Ballasted track interaction effects in railway bridges with simply-supported spans composed by adjacent twin single-track decks, Engineering Structures 247.

[31] C. Bonifácio, D. Ribeiro, R. Calçada, R. Delgado, Dynamic behaviour of a short span filler-beam railway bridge under high-speed traffic, in: Proc. 2nd Int. Conf. on Railway Technology: Research, Development and Maintenance, 2014.

[32] A. Romero, P. Galvín, J. Domínguez, Comportamiento dinámico de viaductos cortos considerando la interacción vehículo-vía-estructura-suelo, Revista Internacional de Métodos Numéricos para Cálculo y Diseño en Ingeniería 28 (1) pp. 55-63 28 (1) (2012) 55–63.

[33] A. Romero, M. Solís, J. Domínguez, P. Galvín, Soil-structure interaction in resonant railway bridges, Soil Dynamics and Earthquake Engineering 47 (2013) 108–116.

[34] K. Nguyen, J. Goicolea, F. Gabaldón, Comparison of dynamic effects of high-speed traffic load on ballasted track using simplified two-dimensional and full three-dimensional model, Journal of Rail and Rapid Transit 228 (2) (2012) 128–142.

[35] CEN/TC256, EN 13674-1:2011+A1:2017 Railway applications - Track - Rail - Part 1: Vignole railway rails 46 kg/m and above, European Committee for Standardization, Brussels, 2017.

[36] M. Melis, Embankments and ballast in high speed rail. fourth part: High-speed railway alignments in spain (1). Certain alternatives [in spanish], Revista de Obras Públicas (3.476) (2007) 41–66.

[37] P. Punetha, S. Nimbalkar, H. Khabbaz, Analytical evaluation of ballasted track substructure response under repeated train loads, International Journal of Geomechanics 20 (7) (2020) 04020093.

[38] Y. Sun, Y. Guo, Z. Chen, W. Zhai, Effect of differential ballast settlement on dynamic response of vehicle–track coupled systems, International Journal of Structural Stability and Dynamics 18 (7) (2017) 1850091.

[39] X. Zhang, C. Zhao, W. Zhai, Dynamic behavior analysis of high-speed railway ballast under moving vehicle loads using discrete element method, International Journal of Geomechanics 17 (7) (2017) 04016157.

[40] R. Ferrara, G. Leonardi, F. Jourdan, A contact-area model for rail-pads connections in 2D simulations: sensitivity analysis of train induced vibrations, International Journal of Vehicle Dynamics and Mobility 51 (9) (2013) 1342–1362.

[41] G. D. Mino, M. D. Liberto, C. Maggiore, S. Noto, A dynamic model of ballasted rail track with bituminous sub-ballast layer, Procedia - Social and Behavioral Sciences 53 (2012) 366–378.

[42] Y. Wang, Z. Dimitrovová, J. Yau, Dynamic responses of vehicle ballasted track interaction system for heavy haul trains, MATEC Web of Conferences 148 (2018) 05004.

[43] P. Museros, E. Moliner, M. Martínez-Rodrigo, Free vibrations of simply-supported beam bridges under moving loads: Maximum resonance, cancellation and resonant vertical acceleration, Journal of Sound and Vibration 332 (2013) 326–345.

[44] J. Haataja, Matlab function for simulating a simple real-coded genetic algorithm., Center for Scientific Computing, Box 405, FIN- 02101 Espoo. Internet:Juha.Haataja@csc.fi (2000).

[45] CITEF, Informe sobre resultado de registros en puente sobre Río Guadiana P.K. 1600.000. Línea Madrid-Cádiz, tramo Alcázar de San Juan - Manzanares. (2005).

[46] J. Manterola, Puentes. Apuntes para su diseño, cálculo y construcción., Colegio de Ingenieros de Caminos, Canales y Puertos, 2006.

[47] A. Zangeneh, C. Svedholm, A. Andersson, C. Pacoste, R. Karoumi, Identification of soil-structure interaction effect in a portal frame railway bridge through full-scale dynamic testing, Engineering Structures 159 (2018) 299–309.

[48] C. Zang, H. Grafe, M. Imregun, Frequency-domain criteria for correlating and updating dynamic finite element models, Mechanical Systems and Signal Processing 1 (15) (2001) 139–155.

[49] K. Matsuoka, K. Kaito, M. Sogabe, Bayesian time–frequency analysis of the vehicle–bridge dynamic interaction effect on simple-supported resonant railway bridges, Mechanical Systems and Signal Processing 135 (2020) 106373.